ministerie van verkeer en waterstaat

**koninklijk nederlands meteorologisch instituut**

# An analytic conceptual model of extratropical cyclones

L.C. Heijboer

Scientific reports; WR 93-03

Wetenschappelijke rapporten; WR 93-03

De Bilt, 1993

De Bilt 1993

Scientific reports = wetenschappelijke rapporten;
WR 93-03

Postbus 201
3730 AE De Bilt
Wilhelminalaan 10
Telefoon 030-206 911
Telefax 030-210 407

UDC: 551.515.1
551.509.3
ISSN: 0169-1651
ISBN: 90-369-2041-8

# An analytic conceptual model of extratropical cyclones

L.C.Heijboer

Royal Netherlands Meteorological Institute
P.O. Box 201,
3730 AE de Bilt,
The Netherlands

## Summary

An analytic conceptual model has been developed describing the nonlinear development of small and large scale extratropical cyclones towards the mature stage.

The model shows the self-development and self-limiting processes of an extratropical cyclone and reveals the existence of A- and B-development, as described by Petterssen and Smebye. Even a so-called ' synoptic bomb ' can be simulated. The model also describes the essential subsynoptic scale features, such as warm and cold frontal zones, together with the associated conveyor belts, as well as the overrunning of the descending high tropospheric and low stratospheric air over the warm conveyor belt, together with the tropopause fold caused by the descending air.

A linear stability analysis has been carried out with the equations. For the unstable modes the results agree with those of the classical linear stability theory for rectangular sine-waves. Asymptotic expressions for the most unstable mode for large time have been obtained for the maximum windspeed of the disturbance and the amount of spiralling of the thermal field as function of the radius, the Coriolis parameter, the layer thickness, the static stability and the thermal wind of the background flow.

Because the analytic solution consists of elementary mathematical functions, the model can easily be run on a personal computer. This, together with the conceptual nature of the model, contributes considerably to the understanding of the behaviour and (sub)synoptic structure of extratropical cyclones and makes the model well suited for educational purposes.

As an application the model has been used for the estimation of the vertical transport of trace gases. Calculations and statistical observational evidence, indicate that in the Northern Hemisphere depressions generate a mean downwards ozone flux from the lower stratosphere of about $5 \times 10^{14}$ molecules ozone per second and squared meter. Moreover, calculated upward vertical velocities suggest that molecules with a residence time of the order of days, originally in the boundary layer, participate in the chemistry of the upper troposphere.

## Contents

## 1. Introduction

At midlatitudes the daily weather and the atmospheric transport of warmth, moisture, momentum and trace constituents are largely determined by the extratropical cyclones (ETC's). Therefore, for a long time, ETC's have been subject to numerous investigations (Reed 1990). These studies can be devided into:
- synoptic studies based on measurements e.g. surface observations, radiosondes, radar, satellites (Browning 1990, Newton 1990)
- theoretical research using the basic physical laws (Hoskins et al. 1985, Hoskins 1990, Eliassen 1990)
- simulations with analytical and numerical models (Hoskins 1990, Shapiro and Keyser 1990)
- daily operational weather prediction which currently has been reached a high standard of performance (Anthes 1990, Bengtsson 1990).

In spite of these extensive research, the knowledge of the processes determining the behaviour of ETC's with its associated air flows is still incomplete. This lack of understanding is due to the complexity and high nonlinearity of the processes determining the evolution of ETC's. Notwithstanding those difficulties, the nonlinear behaviour has been and is accurately simulated by numerous high resolution models e.g. those of Hoskins 1976, Mudrick 1974, and the operational ECMWF-model to name but a few. Though, those simulations and numerical predictions have deepened our insights significantly, the high resolution models are complex and therefore remain difficult to understand. What is lacking up to now is a model, easy to understand, comprising a simple analytic solution giving a conceptual description of relevant processes on ETC's on the (sub)synoptic scales. Such a simplified model, as long as it is able to describe most of the essential features of developing ETC's would contribute considerably to our understanding and would be extremely suited for educational purposes.

In this paper, such a simplified model is presented consisting of an analytic approximate solution of the vorticity and thermodynamic equations and which is also conceptual in the sense that it describes the development, structure and (sub)synoptic air flows of ETC's. Though the model is simple it still is complete to a high degree, namely the main features on subsynoptic scale as they are now understood such as the warm and cold conveyor belts and the downward flow of low stratosphere and high troposphere air overrunning the rising moist warm air and even a kind of tropopause fold are described by the solution. Another important aspect of the model is that it can be easily run with varying parameters and graphical display on personal computers and therefore it is suitable for educational purposes.

The model is described in Chapter 2. It is an extension of an earlier documented prototype (Heijboer 1980a, 1980b). The vertically integrated vorticity and thermodynamic equations used by VIMOLA (Heijboer *et al.* 1989) served as basis for the choice of the components and applied simplifications, because that model runs operationally at the KNMI producing hourly sea-level pressure and wind forecasts on the meso-alpha scales. It has been verified against observations and compared with fine-mesh UKMO forecasts as well. The equations of VIMOLA are equivalent to those of the vertical two-mode model (Flierl 1978, McWilliams 1980) and except for the numerical values of a few constants also with those of the classical two parameter model (Holton, 1992). The approximate solution satisfies a two parameter model based on the semi-geostrophic equations as well, because formulated in geostrophic coordinates they are formally equivalent to the quasi-geostrophic equations (Hoskins and Draghici 1977).

The components of the analytic solution, describing the behaviour of the model, consist of elementary mathematical functions. Starting with a moving circular disturbance of the mean

flow, which has a Gaussian shape and which is either in quasi-geostrophic balance or satisfying the semi-geostrophic relationships, the vertically mean temperature field and the vertically mean velocity fields are described by a sine- and cosine-wave, which move with the circular disturbance and simultaneously are wrapped up by the disturbance. The thermal wind is in quasi-geostrophic or semi-geostrophic balance. The maximum windspeed of the circular disturbance and the angle at which the thermal field is wrapped up around the moving disturbance are described by two nonlinear equations. They are derived from the analytic solution of the integral enstrophy equations for the vorticity of the vertically mean flow and the thermal vorticity of the vertically mean temperature.

Chapter 3 describes the results. Taking representative midlatitude values of the background flow the development as well as the spatial structure of the classical ETC including the 'bomb' are simulated. The model itself indicates some type of A- and B-development (Petterssen and Smebye 1971) and contains the self-development and self-limiting processes of the ETC (Palmen and Newton 1969 P.326 Fig.113).

Calculations of three-dimensional relative streamlines reveal the existence of surfaces which separate seven flow regimes on subsynoptic scale indicating the upward flow in warm and cold conveyor belts and the downward flow of low stratosphere and high troposphere air overrunning the rising moist warm air. The descending air features characteristics of a tropopause fold. The three-dimensional configuration proves to be a useful guide to interprete real cases based on 6-hourly operational ECMWF analyses.

It is shown that, in accordance with simulations of high resolution models, at the lowest pressure level this highly truncated model can reproduce features of the modern conceptual visualization of the cyclone frontal evolution (Shapiro and Keyser 1990).

As an application, the transport of some trace gases by the different flows of the analytical model is treated in Chapter 4. With the aid of statistics of ETC's for the Northern and Southern Hemisphere, using a special approach avoiding the detailed transports in the ETC itself, the total mean downward flux of ozone has been estimated.The flux compares with the computed and observed values (Mahlman *et al.* 1980, Ebel *et al.* 1991). It indicates that ETC's could be responsible for a considerable part of the ozone transport from the stratosphere into the troposphere.

Upward fluxes of a number of trace gases probably important for the chemistry of the upper troposphere have been qualitatively considered leading to a preliminary conclusion that molecules, originally in the boundary layer, with a residence time of the order of days could participate in the chemistry of the upper troposphere.

Discussion and conclusions are presented in Chapter 5.

## 2. Description of the model

*(a) Basic equations*

The classical two parameter model contains the basic equations describing baroclinic instability. They are the vorticity and thermodynamic equation including surface friction and are written in rectangular coordinates x,y,p on the f-plane. The f-plane approximation is justified because the main air flows in extratropical cyclones occur on scales smaller than 2000 km. The vorticity equation reads,

$$\partial_t(\Delta\psi_m) + J(\psi_m, \Delta\psi_m) + G_1 \cdot J(\psi_T, \Delta\psi_T) + f_o \cdot K_f/dp \cdot \Delta\psi_s = 0, \qquad (1)$$

the equation for the thermal vorticity is given by

$$\partial_t(\Delta\psi_T) + J(\psi_m, \Delta\psi_T) + J(\psi_T, \Delta\psi_m) \\ -2 \cdot f_o/(dp \cdot G_2) \cdot \omega_m - f_o \cdot K_f/(dp \cdot G_2) \cdot \Delta\psi_s = 0, \qquad (2)$$

and the thermodynamic equation by

$$\partial_t(\psi_T) + J(\psi_m, \psi_T) - \sigma^* \cdot dp/(2 \cdot f_o) \cdot \omega_m = 0, \qquad (3)$$

with

$$J(a,b) \equiv \partial_x a \cdot \partial_y b - \partial_y a \cdot \partial_x b. \qquad (4)$$

At the lowest surface where $p = p_s$ the geopotential height $z_s$ and the streamfunction $\psi_s$ satisfies

$$z_s = z_m - z_T \text{ and } \psi_s = \psi_m - \psi_T. \qquad (5)$$

When $\psi$ is quasi-geostrophic and depends linearly on p then for $G_1 = 1/4$ and $G_2 = 1/2$ the two-parameter model of Holton (1992) results. Taking $G_1 = G_2 = 1/3$ (1), (2) and (3) are equivalent to those of the vertical two-mode model (Flierl 1978, McWilliams 1980) and the vertically integrated equations of VIMOLA (Heijboer, 1989).

Two other approaches are possible namely a hybride version and one based on the semi-geostrophic equations. In stead of being quasi-geostrophic, $\psi_m$ can satisfy the nonlinear balance equation

$$f_o \cdot \Lambda\psi_m - 2 \cdot \{(\partial_{xy}\psi_m)^2 - \partial_{xx}\psi_m \cdot \partial_{yy}\psi_m\} = g \cdot \Delta z_m , \qquad (6)$$

while $\psi_T$ remains quasi-geostrophic satisfying

$$\psi_T = g \cdot z_T / f_o . \qquad (7)$$

Another alternative is the semi-geostrophic approach of Hoskins and Draghici (1977). Defining the geostrophic coordinates

$$X = x + v_g/f_o \quad , \quad Y = y - u_g/f_o \text{ and } P = p \tag{8}$$

and taking for the streamfunction

$$\psi = \{g.z + (u_g^2 + v_g^2)/2\}/f_o, \tag{9}$$

the same equations results when $\omega_m$ is divided by, and $\sigma^*$ multiplied by the factor $\{1+(\partial_x v_g - \partial_y u_g)/fo\}$. Thus in the semi-geostrophic case $\sigma^*$ is a measure for the potential vorticity rather than the static stability. The semi-geostrophic approach has the advantage that ageostrophic advection, important for frontogenesis, is implicitly taken into account. Moreover, a distinction is made between areas of positive and negative vorticity for the value of $\omega_m$.

$K_f$ is the constant of surface friction in the boundary layer, which is either fixed or proportional to the maximum windspeed of the disturbance as described in the next section.

$\sigma^*$ is a constant value of the effective static stability. It equals the static stability of the dry atmosphere in the case that $\omega \geq 0$ or $q < q_s$. However, if the intensity of the precipitation is $\geq 1$ mm/hr (Phillips 1963) the release of latent heat has to be taken into account. Such intensities frequently occur in ETC's. In that case for which $\omega < 0$ and/or $q \geq q_s$

$$\sigma^* = \sigma - \sigma_{s.ad.} \tag{10}$$

with $\sigma_{s.ad.}$ a constant value of $\sigma$ belonging to the saturated adiabatic lapse rate. The net effect is a lower value of $\sigma$ if latent heat is released. It is noted that in the semi-geostrophic case $\sigma^*$ is a measure for the moist potential vorticity when precipitation occurs.

*(b) Approximate analytic solution*

Where the treatment of the mature midlatitude depression by Holton (1992) is only qualitative, in this section an analytic solution is given enabling a fairly complete quantitative description.

For this the streamfunction $\psi_m$ of the flow at the middle level $p_m$ is split up into a background flow with constant speed $U_m$ equal to the velocity of the moving cyclone and a radial disturbance $\psi_d$. This approach is justified because ETC's are fairly radially symmetric at the middle level.

$$\psi_m = - U_m \cdot y + \psi_d(r_1, t), \tag{11}$$

with

$$\psi_d(r_1, t) = -r_m \cdot v_m(t) \cdot E(r_1), \tag{12}$$

$$r_1 = r/r_m, \quad r = \sqrt{\{(x - U_m \cdot t)^2 + (y)^2\}}, \tag{13}$$

$$E(r_1) = \exp[\{-(r_1)^2 + 1\}/2] = \exp[\{r_m^2 - (x - U_m \cdot t)^2 - y^2\}/(2 \cdot r_m^2)]. \tag{14}$$

$r_m$ is the radius for which the windspeed $v = \partial_r(\psi_d)$ equals the maximum value $v_m$. In the semi-geostrophic case x and y have to be replaced by the geostrophic coordinates X and Y, respectively.

Following James (1950) and McWilliams and Flierl (1979), for the disturbance $\psi_d$ a Gaussian shape was chosen. For $r_1 \leq 2r_m$, this resembles solutions obtained by Flierl (1979) for baroclinic solitary waves with radial symmetry. A Gaussian profile compares reasonably with the shape of mature depressions observed on synoptic weather maps. As is shown in the Appendix the elementary exponential function (14) enables a simple analytical evaluation of the integral enstrophy equations derived from (1) and (2) which were used to determine the equations for $v_m$ of the disturbance and $\phi_m$ of the thermal field.

In the case the streamfunction of $\psi_d$ is quasi-geostrophic the geopotential height $z_d$ of the disturbance becomes

$$z_d = f_o/g \cdot \psi_d \tag{15}$$

either after the substitution into the nonlinear balance equation (6)

$$z_d(r_1,t) = f_o/g \cdot \psi_d(r_1,t) - 1/(2 \cdot g \cdot r_m^2) \cdot \{f_o/g \cdot \psi_d(r_1,t)\}^2. \tag{16}$$

It is easily shown that for constant $v_m$, (11) satisfies the barotropic vorticity equation $\partial_t(\Delta\psi_m) + J(\psi_m, \Delta\psi_m) = 0$, which is a reasonable prognostic equation for the flow at 500 mb on the scale of midlatitude depression for a couple of days ahead. Moreover, for a barotropic atmosphere a circular disturbance like (11) with constant $v_m$ satisfying the nonlinear balance equation is an exact solution of the complete set of inviscid primitive equations in x, y, p-coordinates.

The description of the thermal field needs special attention because the development of the ETC depends on the evolution of that field. Looking for a simple mathematical expression, synoptic weather maps reveal that the thermal pattern (warm and cold tongues in the thickness field 500-1000 mb) of developing cyclones is wrapped up by their cyclonic circulation. However, it is noted that in developing ETC's the horizontal temperature advection is opposed by an increasing value of $\omega_m$ (Palmen and Newton 1969 Pp. 326). In the mature stage the development is stopped by the effect of the vertical velocity and the thermal pattern will move without appreciable change of shape with the velocity of the depression. In that case the thermodynamic equation (3) becomes $\omega_m = 2 \cdot f_o/(\sigma^* \cdot dp) \cdot J(\psi_d, \psi_T)$. Thus, a suitable parametrisation of $\omega_m$ is suggested by the assumption that it is time-dependent proportional to the advection of the thermal field $\psi_T$ by the disturbance $\psi_d$. Proposing that $\omega_m$ satisfies

$$\omega_m = \{1-k(t)\} \cdot 2 \cdot f_o/(\sigma^* \cdot dp) \cdot J(\psi_d, \psi_T) \tag{17}$$

after the substitution into (3) it follows that

$$\partial_t \psi_T = - k(t) \cdot J(\psi_d, \psi_T). \tag{18}$$

It should be stressed that though (18) is a reasonable descriptive equation for the mean thermal

field (thickness 500-1000mb), it is certainly not generally applicable for the temperature at arbitrary levels where the detailed vertical temperature advection play a role.

Concerning k, it appears that it is positive between 0 and 1. During the development it decreases towards k=0 in the mature stage.

A simple mathematical function for $\psi_T$ describing the spiral form of the warm and cold tongues is a single sine-wave like

$$\psi_T = - U_T \cdot g(r_1,t) \cdot \sin\{\phi - h(r_1,t)\}. \tag{19}$$

The functions g and h are prescribed by the demands of eqs. (12) and (18) and the initial condition that at t=0, $\psi_T$ satisfies the uniform thermal background flow

$$\psi_{Tbackground} = - U_T \cdot y = - U_T \cdot r_m \cdot r_1 \cdot \sin(\phi). \tag{20}$$

Substituting (19) into (18), using (12) and (20) result in

$$g(r_1,0) = g(r_1,t) = r_m \cdot r_1, \tag{21}$$

and

$$h(r_1,0) = 0, \quad h(r_1,t) = \phi_m(t)\, E, \tag{22}$$

with

$$\partial_t \phi_m = k(t) \cdot v_m(t)/r_m. \tag{23}$$

Thus, $\psi_T$ consists of a sine-wave moving around the translating disturbance $\psi_d$ with an angular speed depending on radius $r_1$. For $r = r_1$, $E(r_1) = 1$ and the angular velocity equals $\partial_t \phi_m$. For $r_1 \rightarrow \infty$ with $E(r_1) \rightarrow 0$, $\psi_T$ satisfies the background thermal field.

It is noted that for values of $U_T$, $r_m$ and $\phi_m$ representative for midlatitude cyclones the computed patterns according to (19) typically resembles those of the thickness 500-1000 mb fields in developing cyclones.

To close the solution, the maximum windspeed $v_m$ of $\psi_d$ and the angle $\phi_m$ have to be determined as function of time. Synoptic experience shows that an enstrophy cascade takes place in developing cyclones by the elongation of the thermal vorticity patterns. Therefore, it is required that the solution satisfies the integral enstrophy equations for $\psi_d$ and $\psi_T$. The derivation is given in the Appendix. The resulting equations for $v_m$ and $\phi_m$ read:

$$\partial_t v_m = 3/2 \cdot G_1 \cdot U_T^2 / r_m \cdot \phi_m - f_o \cdot K_f/dp \cdot v_m, \tag{24}$$

with $K_f$ dependent on $v_m$ according to

$$K_f = K_{fr} \cdot |v_m| \tag{25}$$

and a constant value is taken for $K_{fr}$.

$$\partial_t\phi_m = \{(K_{mod}\cdot r_m^2 - 3)\cdot v_m/r_m - f_o\cdot K_f/(dp\cdot G_2)\cdot(3\cdot\phi_m+3/16\cdot e\cdot\phi_m^3)\}$$

$$/(K_{mod}\cdot r_m^2 + 3 + 3/8\cdot e\cdot\phi_m^2), \qquad (26)$$

with the model's constant $K_{mod}$ given by

$$K_{mod} = 4\cdot f_o^2/(dp^2\cdot\sigma^*\cdot G_2). \qquad (27)$$

The validity of the approximate solution was tested by comparing it with the results of a numerical time-integration of the complete set (1), (2) and (3) starting with $v_m$=20 ms$^{-1}$ and $\phi_m$=0 as initial conditions with and without surface friction included (constant $K_f$) showing fair agreement for about one day in advance. An example is given in Chapter 3 which describes the results. The model shows that the thermal field, mean vertical velocity and the geopotential height field $z_s$ at sea level exhibits the structure of the classical well developed ETC (Palmen and Newton Pp. 326 Fig.113). This is fairly consistent with numerous examples derived from synoptic weather maps and satellite images with respect to the locations of the vertical velocity pattern, the thermal field and the pressure pattern at sea level showing the through, bent-back warm frontal zone with the maximum windspeeds and the cold frontal zone.

*(c) Stability analysis*

A stability analysis is carried out on the linearized equations (24) and (26). Assuming a frictionless atmosphere ($K_{fr}$ = 0), a small amplification (small $\phi_m$) of the thermal wave, (24) and (26) can be linearized and become

$$\partial_t v_m = C_v\cdot\phi_m, \quad \partial_t\phi_m = C_\phi\cdot v_m, \qquad (28)$$

with

$$C_v = 3/2\cdot G_1\cdot U_T^2/r_m, \; C_\phi = (K_{mod}\cdot r_m^2 - 3)/\{(K_{mod}\cdot r_m^2 + 3)\cdot r_m\}. \qquad (29)$$

Under these assumptions a stability analysis can be carried out for an initial disturbance $\psi_d$ with a finite amplitude. It can be noted that (28) also holds with friction if $v_m$ of the initial disturbance is small. Assuming the solution

$$v_m(t) = v_m(0)\cdot\exp(\omega_f\cdot t), \quad \phi_m(t) = \phi_m(0)\cdot\exp(\omega_f\cdot t), \qquad (30)$$

the frequency $\omega_f$ has to satisfy

$$\omega_f = \pm\sqrt{(C_v\cdot C\phi)}. \qquad (31)$$

Unstable solutions exists for $K_{mod}\cdot r_m^2 > 3$ and stable oscillating solutions for $K_{mod}\cdot r_m^2 < 3$. The

most unstable mode (maximum $\omega_f$) is found for

$$K_{mod} \cdot r_m^2 = 3 + 3\sqrt{2} \, . \tag{32}$$

The ratio of the amplitudes of the solutions for the most unstable radius $r_m$ satisfies

$$v_m(0)/\phi_m(0) = \pm \sqrt{(C_v/C_\phi)} = \pm 1/2 U_T \sqrt{(2+2\sqrt{2})}. \tag{33}$$

The instability of isolated vortices has been studied by McWilliams and Gent (1986) and Flierl (1988). They show that a circular barotropic disturbance is unstable to a sinusoidal perturbation in the thermal field if it is big enough compared to the deformation radius $r_m$ here given by $K_{mod} \cdot r_m^2 = 3$.

The unstable circular modes are excited by the baroclinic instability of the background flow in the same manner as the unstable sinusoidal perturbations of the classical stability analysis. This has been investigated by linearizing (1) and (2). After the substitution of a rectangular sine-wave with wavelength $L_y$ and $L_x$ in the y- and x-direction and assuming that $L_x = 4 \cdot r_m$ the results can be compared with those of the circular disturbance. The agreement is remarkable as well as for the most unstable mode ($K_{mod} \cdot r_m^2 = 3(1+\sqrt{2})$ versus $3.08(1+\sqrt{2})$), the neutral mode ($K_{mod} \cdot r_m^2 = 3$ versus 3.08), the exponential growth ($0.46 \cdot U_T/r_m \cdot t$ versus $0.58 \cdot U_T/r_m \cdot t$) and the ratios of the amplitudes between height and thickness (1.10 versus 0.90).

To explain this agreement it is noted that the total field of $\psi_d$ can be thought to be composed of a series of subsequent circular disturbances in the x-direction with alternating rows of cyclones and anticyclones in the y-direction having a mutual distance of $4 \cdot r_m$ (such a distance assures little mutual interaction). Grouped in that way nearly the same perturbation in the thermal field as for the rectangular sine-wave with $L_y/L_x = 2$ and $L_x = 4 \cdot r_m$ will be forced. See Fig.1 which shows a sketch. Defining now

$$E_{p,q} \equiv (-1)^q \cdot \exp(0.5) \cdot \exp[-\{(x/r_m - 4 \cdot p)^2 + (y/r_m - 4 \cdot q)^2\}/2], \tag{34}$$

$\psi_d$ and $\psi_T$ can be written in a series and, for small $v_m$ and $\phi_m$, can be approximated by a rectangular sine-cosine-wave like

$$\psi_d = -r_m \cdot v_m \cdot \left( \sum_{p,q=0}^{\infty} E_{p,q} \right) \cong -r_m \cdot v_m \cdot \exp(0.5) \cdot 1/2 \cdot \{\cos(2\pi/L_x \cdot x) + 1\} \cdot \cos(2\pi/L_y \cdot y), \tag{35}$$

$$\psi_T = -U_T \cdot y - U_T \cdot [\{\cos\left( \sum_{p,q\ 0}^{\infty} E_{p,q}\ \phi_m \right) - 1\} \cdot y - \sin\left( \sum_{p,q=0}^{\infty} E_{p,q} \cdot \phi_m \right) \cdot x]$$

$$\cong -U_T \cdot y + U_T r_m \cdot \exp(0.5) \cdot \phi_m \cdot \sin(2\pi/L_x) \cdot \cos(2\pi/L_y), \tag{36}$$

with $L_x = 4 \cdot r_m$ and $L_y = 2 \cdot L_x$.

With these approximations the application of the classical linear stability analysis directly leads to the desired results.

*(d) Asymptotic expression for the most unstable mode*

The circular disturbance $\psi_d$ with small intensity ($v_m$ small) is embedded in the background thermal field with constant velocity $U_T$ having a weak wave disturbance ($\phi_m$ small). In that case (28) hold at t = 0 and (24) and (26) predict the nonlinear evolution of $v_m$ and $\phi_m$, respectively.
The asymptotic solution is obtained for large t for which $\partial_t v_m \to 0$ and $\partial_t \phi_m \to 0$. From (24), (25) and (26), using (27) and (32), the following relations for $r_m$, $\phi_m$ and $v_m$ can be found for the radius $r_m$ with the maximum growth rate.

$$r_m = dp/(2 \cdot f_o) \cdot \sqrt{\{\sigma^* \cdot G_2 \cdot (3+3\sqrt{2})\}}, \tag{37}$$

$$1/16 \cdot e \cdot \phi_m^3 + \phi_m = 2\sqrt{(2 \cdot G_2)}/[K_{fr} \cdot \sqrt{\{\sigma^* \cdot (3+3\sqrt{2})\}}], \tag{38}$$

$$v_m^2 = U_T^2/(2 \cdot \sqrt{2}) \cdot G_1/G_2 \cdot (3/16 \cdot e \cdot \phi_m^4 + 3 \cdot \phi_m^2). \tag{39}$$

According to (23) $k(t) \to 0$ for large t because $\partial_t \phi_m \to 0$. Using $k(t)=0$ it follows from (12), (17) and (19) that the minimum value $\omega_{min}$ of $\omega_m$ is found for $r_1 = 1$ and $\phi = \phi_m$ and reads

$$\omega_{min} = -2 \cdot f_o \cdot U_T \cdot v_m/(\sigma^* \cdot dp). \tag{40}$$

The qualitative behaviour of the solution depending on variations in the thermal background flow $U_T$, the effective static stability $\sigma^*$, the constant $K_{fr}$ of the surface friction and the layer thickness dp can be inferred from (37)-(39) i.e. that for the thermal background flow increasing $U_T$ leads to increasing $v_m$ and decreasing $\omega_{min}$, that for the effective static stability decreasing $\sigma^*$ leads to decreasing $r_m$ and increasing $\phi_m$, $v_m$ and decreasing $\omega_{min}$, that for the surface friction decreasing $K_{fr}$ leads to increasing $\phi_m$, $v_m$ and decreasing $\omega_{min}$ and that for the layer thickness decreasing dp leads to decreasing $r_m$ and $\omega_{min}$.

Summarizing

The solution supports the meteorological evidence that:
-Strong spiralling of the thermal field and vertical velocity pattern occur in an environment having low effective static stability and low surface friction.
-Large cyclones of strong intensity can be expected in an environment with strong baroclinic background flow, low effective static stability and low surface friction.
-Small scale cyclones occur in an environment with low effective static stability and small layer thickness.
-Strong vertical velocity occurs with strong baroclinicity, low effective static stability and small layer thickness.

## 3. Results

*(a) Comparison with a numerical integration*

To check the validity of the approximate analytic solution a comparison was carried out with a numerical integration of (1), (2) and (3) using $G_1=G_2=1/3$ formulated in a moving coordinate system with speed $U_m$. The integration was performed using second order difference approximations for the Laplacians and Jacobians and a leapfrog time-stepping scheme with steps of 15 minutes on a square grid consisting of 40x40 points with a grid distance of 75 km. To prevent nonlinear instability, waves with wavelengths of two and three grid distances were removed by applying the smoothing operator developed by Shuman (1957), after every three hours of integration.

The following values fairly representative for occurring midlatitude cyclones were chosen: $g = 9.8\ ms^{-2}$, $f_o = 10^{-4}\ s^{-1}$, $p_u = 2x10^4$ Pa, $p_s = 10^5$ Pa, for the background field a constant $U_m = U_T = 10\ m\ s^{-1}$, for the circular disturbance $r_m = 5x10^5$ m lying in the range for North Atlantic depressions (Dodds 1971). Initial values for $t = 0$ were $v_m(0) = 20\ m\ s^{-1}$ and $\phi_m(0) = 0$. Thus the initial situation consisted of a well developed circular disturbance superposed on a constant uniform baroclinic background field.

The results of the computations depend on the value of the effective static stability. Two values for the static stability parameter $\sigma^*$ were chosen namely $\sigma^* = 2.2x10^{-6}\ kg^{-2}m^4s^2$ and a much lower value $\sigma = 2.2x10^{-7}\ kg^{-2}m^4s^2$. The first is a characteristic climatological midlatitude value for a dry atmosphere having a normal tropospheric stratification. Taking that value, a 36 hours numerical integration showed a solution with little development of the disturbance. Due to the choice of the initial values and no surface friction the stability analysis of Chapter 2 may be applied. It predicts a stable solution because $K_{mod} \cdot r_m^2 = 2.1$ and thus $< 3$. However, in practice it turns out that the effective static stability in extratropical cyclones is lowered in the northwards moving warm moist air due to the release of latent heat and in the southwards moving cold air by the upward transport of sensible heat.

Taking a value for $\sigma^* = \sigma - \sigma_{s.ad.} = 2.2x10^{-7}\ kg^{-2}m^4s^2$ and a representative climatological value $\sigma = 2.2x10^{-6}\ kg^{-2}m^4s^2$ the static stability of the moist adiabat becomes $\sigma_{s.ad.} = 19.8x10^{-7}\ kg^{-2}m^4s^2$. Fig.2 shows the relationship between the average value of the static stability over the layer 350 mb to 850 mb belonging to a moist adiabatic lapse rate as function of the temperature $\theta_s$ at 1000 mb (Heijboer 1977 P.37). As can be seen from Fig.2 the value $\sigma_{s.ad.} = 19.8x10^{-7}\ kg^{-2}m^4s^2$ lies in the range 17°C-23°C. This is in agreement with a study of Kuo *et al.* (1991) who find seven depressions characterised by the fact that the early stage of development was located over the warm ocean in the vicinity of the Gulf Stream with sea surface temperatures ranging from 17°C-23°C. Also Sanders and Gyakum (1980) conclude that the beginning of explosively deepening marine extratropical cyclones, with central pressure falls at sea level of at least 1 Bergeron during 24 hours, is located over relatively warm water along the edge of the Gulf Stream or in the Sargasso Sea in the area between 35°N and 40°N and between 65°W and 75°W.

Concerning the cold air, which is drawn in from the continent over the warm sea by the developing cyclones, a large destabilization of the air can be expected causing a lapse rate approaching that of the dry adiabat.

Studies carried out with numerical models sustain the low effective static stability occurring

in developing cyclones as well. With respect to the influence of the surface fluxes of sensible and latent heat on the lapse rate and therefore on the development, no significant influence is indicated during the rapidly deepening stage (Heijboer 1977, Fantini 1990, Kuo *et al.* 1991). It is likely that the adjustment towards low effective static stability allowing rapid development has already taken place before. Therefore, consistent with the given arguments, for the simulation of a developing extratropical cyclone, numerically as well as analytically, a low but constant value $\sigma^*=2.2\times10^{-7}$ kg$^{-2}$m$^4$s$^2$ was taken for the ascending warm moist air and for the descending cold air as well. For that value an unstable solution can be expected because $K_{mod}\cdot r_m^2=21.3$.

The numerical solution for t=6 hours is represented by Fig.3. The thermal field experiences a wave-like amplification. The $\omega_m$-field (positive and negative) shows the pattern typical of a young developing wave. The configuration resembles well the composite picture of the incipient bomb of Sanders and Gyakum (1980). The figure clearly shows a negative $\omega$ located over the low at sea level characteristic of a developing extratropical cyclone. The integration for t=18 hours is shown in Fig.4(a) (composite picture of thermal field $z_T$, height $z_s$ at 1000 mb and vertical velocity $\omega_m$). The figures clearly show the configuration of the classical well developed extratropical cyclone (Palmen and Newton 1969 P.326 Fig.113). The thermal field is spiralled-shaped with warm and cold tongues. The height of 1000 mb shows the classical trough at the rear of the depression with a low level jet (reverse thermal wind shear). The $\omega$-pattern is consistent showing upward motion over the trough. Downward motion occurs after the cold 'front' and the pattern penetrates toward the low pressure centre as can often be observed from satellite imagery.

The numerical solution of the extratropical cyclone was used as reference for the validity of the analytic approximate solution. Starting from the same initial situation the analytic solution for t=18 hours is given by Fig.4(b) (composite picture of $z_T$, $z_s$ and $\omega_m$). Comparison of Fig. 4(a) with Fig.4(b) shows a reasonable agreement between the numerical integration and the analytic solution.

*(b) Scale dependent behaviour of the asymptotic solution*

In Subsection 2(d) the qualitative behaviour of the asymptotic solution has been discussed. It is interesting to investigate the relationships (37)- (40) more quantitatively. For the numerical values of g, $f_o$, $p_u$ and $p_s$ given in 3(a) the dependence of the solution as function of the radius $r_m$ with the maximum growth rate on variations in $U_T$ and $\sigma^*$ of the background flow was investigated. The surface friction was taken into account. For a value of $K_{fr}$ = 200 kg m$^{-2}$s$^{-1}$ and $v_m$ = 10 m s$^{-1}$, according to (25) $K_f$ = 2000 kg m$^{-1}$s$^{-2}$ in accordance to the experimentally determined constant value used in VIMOLA (Heijboer *et al.* 1989).

A necessary condition for reliability of the results is the requirement that the Rossby number Ro<1 for the quasi-geostrophic solution as well as for the semi-geostrophic solution, since in the latter case when Ro approaches 1 in the semi-geostrophic space the vorticity in the physical space tends to go to infinity (Hoskins and West 1979). For a circular disturbance, Ro is given by

$$Ro = v_m/(f_o\cdot r_m) = v_m/(U_T\cdot f_o\cdot r_m).U_T. \qquad (41)$$

Table 1 shows the upper bounds of $U_T$ for several values of $r_m$ and the ratios $v_m/U_T$. This table

shows the high scale dependency of the solution for the static stability $\sigma^*$, the angle $\phi_m$ at which the thermal field is wrapped up along $r_m$, the ratios $v_m/U_T$ and $\omega_{min}/v_m^2$.

TABLE 1. Scale dependency of the asymptotic solution of Eqs. (34)-(36) as function of the radius $r_m$ for the most unstable mode.

| $r_m$ (km) | $U_T$ (m s$^{-1}$) (Ro<1) | $\sigma^*$ ($10^{-7}$m$^4$kg$^{-2}$s$^2$) | $\phi_m$ | $v_m/U_T$ | $\omega_{min}/v_m^2$ ($\omega_{min}$ mb 24h$^{-1}$) ($v_m$ m s$^{-1}$) |
|---|---|---|---|---|---|
| 1000 | <59 | 25.9 | $81^0$ | 1.7 | -0.5 |
| 500 | <17 | 6.5 | $122^0$ | 2.9 | -1.2 |
| 250 | <5 | 1.6 | $171^0$ | 4.9 | -2.7 |
| 100 | <1 | 0.3 | $252^0$ | 9.3 | -9.0 |

For the typical midlatitude cyclone with $r_m$=500 km and $U_T$=10 ms$^{-1}$ Table 1 shows that $\phi_m$=122$^0$, $v_m$=29 ms$^{-1}$ and $\omega_{min}$=-1000 mb 24h$^{-1}$ which are reasonable values. Small scale vortices such as polar lows with $r_m$=100km are highly wrapped up in the thermal and vertical velocity fields and occur in an environment with low effective static stability $\sigma^*$ and vertical windshear $U_T$ (Businger 1985 1987, Businger and Reed 1989, Emanuel and Rotunno 1989, Rasmussen 1979 1985, Turner et al. 1991).

*(c) Simulation of a bomb*

To simulate the ETC from the initial situation towards the mature stage, Eqs. (24) and (26) were integrated numerically using forward time difference schemes with time steps of 1800 s. Because the final situation is determined by the asymptotic solution,
which can be calculated independently, a check on the accuracy of the numerical computation was possible. Time steps of 1800 s proved to be sufficiently accurate.

The initial situation consisted of a weak disturbance with $v_m$ = 1 m s$^{-1}$ and a uniform thermal background field with constant $U_T$ and $\phi_m$ = 0. The integrations were carried out with varying $U_T$ and varying effectivestatic stability $\sigma^*$. The following numerical values were chosen: g = 9.8 m s$^{-1}$, $f_o$ = $10^{-4}$ s$^{-1}$, $r_m$ = 5x10$^5$ m, $p_u$ = 2.12x10$^4$ Pa, $p_s$ = 1.012x10$^5$ Pa, dp = 8x10$^4$ Pa, $K_{fr}$ = 200 kg m$^{-2}$s$^{-1}$. The lowest level was chosen at the fairly representative climatological value of the surface pressure (1012mb).

At first a run was performed with $U_T$ = 10 m s$^{-1}$ and $r_m$ = 500 km. Assuming for $r_m$ the most unstable radius then according to (27) and (32) $\sigma^*$ must have the value $\sigma^*$ = 6.5x10$^{-7}$ kg$^{-2}$m$^4$s$^2$.

Concerning the central pressure fall the criterion at 45$^0$N for the development of a bomb is a fall of 1 Bergeron during 24 hours which means a $\Delta p$ = 24xsin45$^0$/sin60$^0$ = 19.6 mb/24h (Sanders and Gyakum 1980, Sanders 1986). Thus taking $U_T$ = 10 m s$^{-1}$ and $\sigma^*$ = 6.5x10$^{-7}$ kg$^{-2}$m$^4$s$^2$ only moderate development is achieved typically for a normal ETC. However, using the value for $\sigma^*$ of 2.2x10$^{-7}$ kg$^{-2}$m$^4$s$^2$, which after Subsection 3(a) corresponds better to explosive development, the computed pressure fall strongly increased. The computed pressure

followed the profile for the rapidly developing North Atlantic depressions (Smigielski and Mogil 1991) during a period of 48 hours from t = 90 h to t = 138 h. The central pressure fall given in Fig.5(a) satisfied the bomb criterion of Sanders and Gyakum (1980), although according to the category of intensities applied by Sanders (1986) it was a weak bomb. Fig.5(b) shows the strongly increased development of $v_m$ resulting in a much stronger final windspeed. Fig.5(c) expresses the strongly increased $\phi_m$ in the final stage from $120^0$ to nearly $240^0$.

For the values of $U_T$ = 10 m $s^{-1}$ and $\sigma^*$ = $2.2\times10^{-7}$ $kg^{-2}m^4s^2$ the radius $r_m$= 500 km is not the radius of maximum instability, which occurs for $\sigma^*$ = $6.5\times10^{-7}$ $kg^{-2}m^4s^2$. Demanding the same value of $v_m$ as was computed in the asymptotic case for the run with $U_T$ = 10 m $s^{-1}$ and $\sigma^*$ = $2.2\times10^{-7}$ $kg^{-2}m^4s^2$ then, according to (37), (38) and (39), the corresponding $U_T$ can be computed. It amounts to $U_T$ = 14 m $s^{-1}$. The results for that run are given by the dashed lines in Figs.5(a)-5(c). This leads to the result that the development of the pressure and pressure fall were very similar to those of the run with $U_T$ = 10 m $s^{-1}$ and $\sigma^*$ = $2.2\times10^{-7}$ $kg^{-2}m^4s^2$, but $\phi_m$ and the vertical velocity were a factor two less intense. This outcome can be inferred from (37), (38) and (39) because $\phi_m$ only depends on $\sigma^*$ and $v_m$ is proportional to $U_T$.

Thus a weak bomb was simulated under different conditions namely by the increase of the baroclinicity of the background flow or by the lowering of the effective static stability. In the latter case of a lower effective static stability the shape of the thermal pattern and therefore the pattern of the vertical velocity was more spiralled with accompanying intenser vertical velocities.

*(d) Sensitivity of the analytic solution to the initial conditions*

In Subsection 3(a) the numerical and analytical solution was computed for t = 18 h starting with $v_m$ = 20 m $s^{-1}$ and $\phi_m$ = $0^0$, where in 3(c) for the simulation of the bomb the initial condition was $v_m$ = 1 m $s^{-1}$ and $\phi_m$ = $0^0$. The question arises how sensitively the asymptotic solution depends on the initial values. For that purpose integrations were carried out for different values of $v_m$ with $\phi_m$ = $0^0$ forwards in time towards the asymptotic solution as well as backwards in time.

The calculations were performed with values $U_T$ = 10 m $s^{-1}$, $\sigma^*$ = $2.2\times10^{-7}$ $kg^{-2}m^4s^2$ and $r_m$ = $5\times10^5$ m. The solution showed a hyperbolic character with three equilibrium points namely two stable points consisting of asymptotic solutions for a cyclone and an anticyclone and the origin which was unstable.

Only the trajectories with $v_m \geq 0$ and $\phi_m > 0$ are relevant for developing cyclones and they are shown in Fig.6. All trajectories starting with $\phi_m$ smaller than about $60^0$ and $v_m$ smaller than roughly 10 $ms^{-1}$ rapidly converge indicating no significant difference between cyclones in the stage of rapid development.

The diagram suggests two types of cyclone development namely type A and type B as described by Petterssen and Smebye (1971). Type A-development is located near the positive $\phi_m$-axis. Disturbances starting with small $v_m$ have a disturbed thermal field but little vorticity advection at the middle level. Thus thermal processes tend to dominate initially. Type B-development is associated with disturbances starting near the positive $v_m$-axis with small $\phi_m$. They have appreciable positive vorticity advection at the middle level initially.

Concerning the initial conditions it is noted that the existing initial situation has been arisen from the flow before t=0. Thus in the case of A-development the disturbed thermal field of that special form must have been already created by a disturbed flow. In the case of B-development a circular barotropic disturbance already exists. One can imagine that remnants of earlier disturbances could be responsible for it. Therefore, the B-development seems to be of more practical relevance than the A-development.

It is interesting to note that the analytic solution given in Fig.4(b) with $v_m$ = 20 m $s^{-1}$ and $\phi_m$ =111$^0$ is located in the area where the trajectories converge. Furthermore, it is clear that the start values of $v_m$ = 1 m $s^{-1}$ and $\phi_m$ = 0$^0$ used for the simulation of the bomb nearly coincides with the trajectory starting from the origin towards the asymptotic solution of the cyclone which is in the middle of all converging trajectories.

Numerical integrations revealed a great numerical insensitivity for all calculations forward in time towards the asymptotic solutions. However, starting from the asymptotic solution backwards in time the results were very sensitive to the exact start values and even round off errors were important. These results are also suggested by Fig.6 showing the divergent trajectories from the cyclone.

*(e) Three-dimensional relative streamlines*

Up to now only vertically averaged variables such as the mean height $z_d$, the thermal field $z_T$, the mean vertical velocity $\omega_m$ and the height of 1000 mb $z_s = z_m - z_T$ have been considered.

However, it is possible to get a view of the three-dimensional structure. Therefore, it is assumed that the rotational as well as the irrotational parts of the horizontal wind depend linearly on p. Then using the continuity equation with the boundary conditions $\omega = 0$ for $p = p_u$ and $p = p_s$, the rotational horizontal components u and v and the vertical component $\omega$ dependent on x, y, and t but also on p can be derived. They are given by (A50), (A51) and (A52) in Subsection (b) of the Appendix.

Three-dimensional streamlines relative to the moving cyclone were computed for the analytic solution given in Fig.4(b) with $v_m$ = 20 m $s^{-1}$, $\phi_m$ = 111$^0$. Keeping t constant the computation was carried out with a trajectory program applying the following relationships:

$$dx_1/dt = u(x_1, y_1, p_1, t), \tag{42}$$

$$dy_1/dt = v(x_1, y_1, p_1, t), \tag{43}$$

and

$$dp_1/dt = 2.\omega(x_1, y_1, p_1, t)/(p_s - p_u). \tag{44}$$

with the relative coordinates $x_1$ and $y_1$ given by (A40) and $p_1$ given by (A37). To avoid computational instability the integrations were carried out with a leapfrog scheme with short steps of 324 s (100 steps in 9 hours). Such short intervals yielded sufficiently accurate results.

Due to the existence of separation surfaces seven different flow regimes could be distinguished. They are depicted in Fig.7, which is a qualitative three-dimensional view of the

channel from west to east in which the cyclone is embedded. To distinguish stratosphere air from troposphere air in the model it was crudely assumed that a 'tropopause' is situated at 300 mb in the western part of the channel. The seven flows are:
1 Warm moist conveyor belt with inflow at the eastern side in the boundary layer and outflow in the high troposphere at the eastern side,
2 Flow of the environment only slightly influenced by the depression with inflow at the eastern side in the low troposphere and outflow at the western side in the low troposphere,
3 Cold moist conveyor belt with inflow at the eastern side in the boundary layer and outflow at the western side in the boundary layer,
4 Descending low stratosphere air and high troposphere air overrunning the warm conveyor belt with inflow at the western side and outflow at the eastern side of the cyclone,
5 Flow of the environment influenced only slightly by the depression with inflow at the western side in the low stratosphere and high troposphere and outflow at the eastern side in the low stratosphere and high troposphere,
6 Descending low stratosphere air and high troposphere air into the boundary layer of the troposphere with inflow and outflow at the western side,
7 Circulating air in the core of the cyclone upwards and downwards and moving with the speed of the cyclone.

Trajectory calculations show that the updraught from the low troposphere to the high troposphere takes place in about one day. Flow 1 features some characteristics of the warm conveyor belt documented by Green *et al.* (1966), Browning and Harrold (1970), Harrold (1973), Carlson (1980), Browning (1985, 1990). The air of flow 3 is under flow 1 and moves upwards towards above 400 mb around the cyclone on the northern side while it is moistened by the falling precipitation of flow 1. At the western side of the cyclone it moves outwards and downwards. This suggests characteristics of a cold conveyor belt (Carlson 1980, Ludlam 1980, Browning 1985, 1990). The pattern of upward motions compares with those of satellite images of synoptic scale cloudiness of well developed ETC's. The air of flow 4 originating from the low 'stratosphere' and high troposphere moves eastwards and downwards on the southern side of the cyclone. On the eastern side it moves sharply upwards overrunning the air of flow 1. It indicates the overrunning of a warm conveyor belt (Miles 1962, Browning and Monk 1882, Browning 1985, 1990). The descending air of 4 and 6 originating from above 300 mb featured a funnel of a tropopause fold. The funnel had horizontal width of 100 to 200 km, the shape and the spatial dimensions are not contradicted by theoretical and observational studies (Reed 1955, Danielsen 1968, Hoskins and Bretherton 1972, Shapiro 1980, Uccellini *et al.* 1985, Ebel *et al.* 1991).

*(f) Lagrangian evolution of the thermal field near sea level*

It is shown in this subsection that the analytic solution features the conceptual model of the structural evolution of the surface thermal field characteristic of developing marine ETC's as described by Shapiro and Keyser (1990). Therefore, the thermodynamic equation with the assumption that $\omega=0$ is applied at the pressure level just above the friction layer. Then the temperature $T_s$ at $p=p_s$ is completely determined by the horizontal advection

$$\partial_t T_s + u_s \cdot \partial_x T_s + v_s \, \partial_y T_s = 0. \tag{45}$$

Using the analytic expression for u and v given by (A50) and (A51) for $p=p_s$ ($p_1=1$), a

Lagrangian integration of (45) can be easily performed. This has been carried out using the trajectory program described in Subsection 3(e) for the x- and y-coordinates of the points of a mesh consisting of 30x30 grid points with d=100km. They were integrated backwards in time to t=0 where the corresponding values of $T_s$ for t=0 belonging to the field given by (20) were picked up. A number of integrations were carried out using different initial values of $v_m$ at t=0. All runs showed features of the evolution of the surface thermal field typical for developing marine ETC's such as frontal fracture, bent-back warm frontal zone at the mid point of cyclogenesis and a warm-core seclusion in the post-cold frontal air within the mature, fully developed cyclone. An example is given by Figs.8(a)-8(d) showing the evolution of the isobars and of the thermal field near sea level, starting at t=0 in Fig.8(a). Subsequent figures are in steps of 12 hour, showing the well developed cold front, warm conveyor belt, frontal fracture and bentback warm frontal zone (Fig.8(d)). These figures were produced with the software package of the model, which runs on an IBM compatible personal computer. Evolutions like this with varying background flow parameters can be handled easily. It illustrates the feasibility of the model for educational instruction.

## 4. Application to the transport of trace gases

At KNMI 6-hourly ECMWF analyses are being used for research on the transport of trace gases whose vertical distribution is important for the radiation balance in climate models. It proved that the conceptual picture of the flow regimes of Fig.7 of the analytical model was very useful to interpret the results of the analyses for the detection of the flow regimes in cases with developing ETC's. In this chapter an application of the model with respect to the transport of some trace gases is described.

### *(a) Scale dependency of vertical velocity and statistics of depressions*

The vertical distribution of trace gases is determined by sources, sinks, chemical reactions and by atmospheric transport. Unfortunately, the knowledge of vertical transport is far from complete. Contrary to the horizontal transport the vertical movements are sensitively scale dependent i.e. the vertical velocity is roughly inversionally proportional to the horizontal scale of the disturbance ranging from 0.1 cm/s for planetary waves to several meters in cumulonimbi. A sensitive scale dependency was also displayed by the analytical model.

For tropospheric chemistry models a regular large scale upward movement of w=0.00015 m $s^{-1}$ is assumed (Hidalgo and Crutzen 1977, Warneck 1988). This leads to a time scale of vertical transport through the troposphere of 20 months. For eddy transport a value of K=15 $m^2$ $s^{-1}$ is not unusual (Hidalgo and Crutzen 1977). This leads to 1 month's time for transport from the boundary layer to the tropopause. However, a large part of vertical transport through the troposphere at midlatitude is not gradually and slow. As will be argued below it occurs rapidly and organised. Migrating ETC's embedded in the large-scale circulation (Gross-Wetter-Lage) play a key role in the rapid vertical transport through the whole troposphere and in the vertical exchange between the troposphere and the lower stratosphere at moderate latitudes. As was indicated by the analytical model and confirmed by observations, ETC's contain a couple of downward and upward airstreams i.e. low stratospheric air and high tropospheric dry air move downward on the backside of the moving depression causing a tropopause fold, while moist warm low tropospheric air moves upward on the frontside of it into the high troposphere pushing the tropopause upward. The characteristic exchange takes place on a time of one to two days.

To obtain an impression of the impact of ETC's on the global transport of trace gases first the available statistics have to be considered. A number of studies are devoted to the statistics of ETC's (Pettersen 1956, Dodds 1971, Kletter 1972, Viezee *et al.* 1983, Nielsen and Dole 1991). The results of Kletter for the frequency of occurrence and cyclonic tracks of ETC's for the Northern and Southern Hemisphere, separated for the four seasons are given in Table 2.

TABLE 2. Frequency of occurrence of cyclonic tracks in the Northern and Southern Hemisphere for the four seasons after Kletter (1972).

| | jan-march | april-june | july-aug | sept-dec | total |
|---|---|---|---|---|---|
| NH | 57 | 45 | 34 | 44 | 180 |
| SH | 52 | 29 | 53 | 91 | 225 |
| Total over the whole earth | | | | | 405 |

Dodds has studied depressions in an area bounded by latitudes 40°N and 65°N and longitudes 40°W and 40°E for the years 1965, 1966 and 1967. He found that at the maximum depth, the depressions per year are distributed as follows: 67 atlantic, 9 Europe and 20 mixed. Thus totally 96 cyclones per year in the domain indicated above. From Kletter's analysis it can be deduced that the North Pacific contains roughly two times as many cyclones as the North Atlantic. That means that the number of Dodd's cyclones can be roughly multiplied by a factor of 3 obtaining for the whole Northern Hemisphere 288 cyclones.

Kletter has found that in the Northern Hemisphere cyclones move from around 40°N towards about 60°N at the the West coast of the USA and Europe. In the Southern Hemisphere he found that cyclones move nearly zonally between 40°S and 60°S and the longitudinal distribution is also rather homogeneous.

Viezee and Johnson estimates the number of cyclones for the Northern Hemisphere to be about 365 in a year that is one per day.

The mean radius of ETC's ranges from 200 to 2000 km (Nielsen and Dole 1991).

*(b) Estimation of the mean downward transport of ozone from the lower stratosphere to the troposphere*

The downward transport of ozone could be calculated for each pressure level by multiplying the mass flux with the mass mixing ratio of ozone. However, in view of the highly truncated two-parameter model based on either the quasi-geostrophic or semi-geostrophic equations, such an approach is not very appropriate and probably leads to inaccurate results. A more attractive manner is suggested by the streamlines' calculations treated in Subsection 3(f). The results of these calculations are not contradicted by the observations. Thus, at least qualitatively, the calculated air flows are correct and suggest that a developing depression consists of an increasing number of rotating air particles drawn in from the environment forming a translating system. A part of these particles originate from the lower stratosphere and another larger part from the troposphere. With respect to ozone, only the total number of molecules drawn in from the stratosphere towards the troposphere for each depression separately has to be estimated and the detailed transport in the depression itself does not matter. This number can be estimated by looking in the western part of the channel where the surfaces separating the air flows are still undisturbed.

To keep the problem simple it has been assumed that the stratospheric air is separated by the tropospheric air by the 300 hPa surface, but it must be noted that similar estimates can be carried out taking a more realistic sloping tropopause. The stratospheric air in the channels 6 and 4 of Fig.7 is caught in and pushed downwards in the depression. A part of this air is drawn into the core and eventually mixed with tropospheric air. Stratospheric air in flow 6 will be deposited in the lower troposphere and the boundary layer, while the stratospheric air of flow 4 represents transport from the lower stratosphere into the upper troposphere and partly back into the lower stratosphere.

Consider first channel 6. The streamline calculation of Subsection 3(f) indicated a width of 800 km and a height of about 1.5 km for the air stream with a relative forward movement of 10 $ms^{-1}$. Taking an ozone concentration of $3.0 \times 10^{18}$ mol $m^{-3}$ at 300 hPa and 50°N (Komhyr et al. 1989) a quantity of $3.6 \times 10^{28}$ mol per second is sucked in in channel 6. The deposition will take place one or two days after the passage of the depression. This is supported by observations (e.g. Wakamatsu et al. 1989). Assuming that the effective downward transport takes place during half of the characteristic total life-time of four days of the cyclone, the total transport per

depression in channel 6 is about $6.2 \times 10^{33}$ molecules ozone.

For channel 4, with a larger width of 1000 km because it occupies a larger part at 300 mb and a same thickness of 1.5 km as for channel 6 and a same relative velocity of 10 $ms^{-1}$, the transport amounts to $4.5 \times 10^{28}$ mol $s^{-1}$. Assuming again an effective downward transport during 2 days, $7.8 \times 10^{33}$ molecules ozone per second are caught in. However, a fraction of these molecules will return into the lower stratosphere. This fraction is dependent on the height differences between the tropopauses ahead and behind the depression and the amount of mixing by convection and shear instabilities between channel 4 and 1. That fraction is taken to be 0.5.

Channel 7 represents the flow in the core. Assuming for the core a characteristic radius of 500 km near 300 mb and a thickness of 1.5 km of stratospheric air which has been caught in and will be mixed with tropospheric air, a total number of $3.5 \times 10^{33}$ molecules ozone is mixed. This number compares with a value of $2.5 \times 10^{33}$ mol ozone per day according to Vaughan and Price (1990).

The total number of ozone molecules drawn in by an ETC is the sum of channel 6 ($6.2 \times 10^{33}$) plus channel 4 ($3.9 \times 10^{33}$) plus channel 7 ($3.5 \times 10^{33}$) summing up to $1.36 \times 10^{34}$ ozone molecules.

For a number of 4 separate depressions per 4 days (Viezee *et al.* 1983), that is effectively one depression per day, for the Northern Hemisphere a number of $5.0 \times 10^{36}$ molecules ozone per year is sucked downwards into the troposphere. This corresponds to a mean vertical ozone flux of $6.2 \times 10^{14}$ mol $m^{-2}s^{-1}$. The result compares with the values commonly assumed for the Northern Hemisphere from $4 \times 10^{14}$ to $10 \times 10^{14}$ mol $m^{-2}s^{-1}$ (Mahlman *et al.* 1980, Ebel *et al.* 1991). Taking 180 cyclones per year for the Northern Hemisphere (Kletter 1972) a lower flux of $3.1 \times 10^{14}$ mol $m^{-2}$ $s^{-1}$ results.

The above simple estimate gives not only an idea about the benefit of the analytical model, when properly used, but also about the importance of the ETC's for the transport of trace gases from the lower stratosphere to the troposphere.

*(c) Estimation of upward fluxes*

For vertical transport around a depression the time scale for upwards transport is about one day and for downward transport about two days. The difference is due to the effect of the release of latent heat in the ascending air.

The air in the boundary layer and lower tropospheric air in the warm moist conveyor belt represents a channel of sucking with a width of about 500 km and a height of 1 km and a relative velocity of 10 $ms^{-1}$. Suppose a trace gas with a concentration of n mol $m^{-3}$. That means a flux of $nx5x10^{9}$ mol $s^{-1}$. Suppose a chemical time scale longer than one day and a depression with an active pumping time of two days. Such a depression transports $8.64 \times 10^{14}$xn molecules. Suppose one day for air to travel upwards from the boundary layer up to the upper troposphere. In one day the horizontal displacement of a standard cyclone is (10 m $s^{-1}$ taken as mean velocity) about 850 km. Therefore, due to the movement of the cyclone, the boundary layer air is deposited in the upper troposphere roughly 1000 km away from the place of the intake in the direction of the track of the depression and ahead of the depression. Hence, trace gases with life times of hours to days participate in the chemical processes of the upper troposphere. Table 3 lists a number of trace gases probably important for the chemistry in the upper troposphere.

TABLE 3. Trace gases important for the chemistry in the upper troposphere.

| tracer | name | residence time |
|---|---|---|
| CO | carbonmonoxide | 10 days-several months |
| $H_2O$ | water vapour | 8 days |
| $C_2H_4$ | etheen | 1 day |
| HCHO | formaldehyde | three hours |
| $NO_x(NO+NO_2)$ | odd nitrogen | 2 days |
| PAN | peroxyacetylnitrate | 1 day-1 month |
| $NH_3/NH_4^+$ | ammoniak/ammonium | 10 days |
| $SO_2$ | sulphurdioxide | 2 days |
| $HNO_3$ | nitricacid | 1 day |
| $CS_2$ | carbondisulfide | weeks |
| Aerosols | | < 5 days (radius $10^{-3}$ - $10^2$ $\mu$m) |

ETC's occur most frequently and are most intense above oceans. The rapid transport of cyclones from the boundary layer and lower troposphere to the upper troposphere implies that good agreement should exist between the mixing ratios of the marine boundary layer and the upper troposphere. This is illustrated in Table 4 (Warneck 1988). The drop of a factor 3 of HCHO could be understood from the relative short lifetime of three hours.

TABLE 4. Mixing ratios (ppbv) of trace gases in the boundary layer and the upper troposphere (Warneck 1988).

| | boundary layer | | upper troposphere |
|---|---|---|---|
| tracer | marine | continental | |
| CO | $1x10^2$ | $2.5x10^2$ | $1x10^2$ |
| $NO_2$ | 0.03 | 2 | 0.03 |
| $SO_2$ | 0.05 | 2 | 0.05 |
| HCHO | 0.3 | 2 | 0.1 |
| $NH_3$ | 0.1 | 4 | 0.1 |

Interesting for the chemistry is that a part of channel 1, the warm moist conveyor belt, mixes up with dry stratospheric air. This is due to mixing processes by instabilities, convective and shear, and/or gravity waves generated at the bifurcation surfaces between the two channels. The jump in velocity and temperature across this surface may lead to Kelvin-Helmholtz instabilities (e.g. Kelder and Teitelbaum 1991) and these instabilities generate mixing. The ozone rich stratospheric air can accelerate chemical reactions through enhanced OH production. This is a consequence of enhanced $O(^1D)$ production by ozone photolysis followed by the reaction $O(^1D) + H_2O \rightarrow 2OH$. To complicate things further the involved tropospheric air is moist or even saturated that means that part of the chemistry changes to wet chemistry.

Moreover, in channel 4 cirrus may be formed leading to heterogeneous chemistry in that region. That means that air of stratospheric and troposperic origin mixed during one to two days and reacting with complex chemistry returns 'processed' to the lower stratosphere and the upper troposphere.

For a cut-off low some comparable chemical consequences of the mixing of stratospheric and tropospheric air have been discussed in Bamber *et al.* (1984).

Another point of importance is that clouds exist in both the warm and cold conveyor belt. That means that lower tropospheric and boundary layer air is pumped through a cloudy environment. During one or two days wet chemistry occurs in these air masses and then the air in the cold conveyor belt returns into the the lower troposphere while the warm conveyor belt put the air into the upper troposphere and perhaps the lower stratosphere. Moreover in both conveyor belts precipitation takes place. Hence certain species will be removed by wet deposition during the transport and deposited on the ground or in underlying atmospheric layers.

## 5. Discussion and conclusions

It is concluded that with the derived simple analytic solution most of the essential characteristics of developing ETC's including the (sub)synoptic air flows can be described conceptually. The solution resembles qualitatively observational studies and high resolution integrations as presented in the literature. The special kind of simplification applied in the model contributes considerably to an easy understanding of the behaviour and (sub)synoptic structure of the ETC and is well suited for educational purposes because the model can be easily run with varying parameters and graphical display on personal computers.

The model consists of two nonlinear equations, one for the maximum wind speed $v_m$ of the circular disturbance, and the other for the angle $\phi_m$ at which the thermal field is differentially wrapped up. The solution contains the self-development and self-limiting processes of the ETC (Palmen and Newton 1969 P.326 Fig.113). The scale dependent structure of the asymptotic solution for large time (Subsections 2(d) and 3(b)) is not contradicted by the observational and theoretical evidence i.e. that strong spiralling of the thermal field and vertical velocity pattern occur in an environment having low effective static stability and low surface friction, that large scale cyclones of strong intensity can be expected in an environment with strong baroclinic background flow, low effective static stability and low surface friction, that small scale cyclones occur in an environment with low effective static stability and small layer thickness, that strong vertical velocity occurs with strong baroclinicity, low effective static stability and small layer thickness.

The trajectories of the analytic solution in the $v_m$-$\phi_m$ space indicate two types of cyclone development namely type A and type B as described by Petterssen and Smebye (1971). Although for type A the initial relative vorticity of the mean flow is small, due to the relative vorticity in the thermal field there is advection of positive vorticity above 600 mb in agreement with the comment of Uccellini (1990 P.86).

In the initial development stage the solution displays a case-to-case variability, but not in the mature stage. That agrees with the statement of Petterssen: 'ETC's are born in a variety of ways, but their appearance at death is remarkably similar' (Uccellini 1990 P.100).

Calculations of relative streamlines of a stationary moving cyclone and calculations of trajectories of a developing cyclone towards the mature stage reveal the existence of seven relative flow regimes separated by bifurcation surfaces which, in case of the developing cyclone change in time. The regimes are characterised by two flows of the environment only slightly influenced by the depression, by two upward flows around the core of the depression, one ending in the upper troposphere (warm moist conveyor belt), and the other flowing northwards and westwards around the depression descending back from the middle troposphere into the boundary layer (cold moist conveyor belt), by two downward flows from the low stratosphere and the high troposphere around the core of the depression, one ending in the boundary layer, and the other participating in the return flow over the warm conveyor belt to the upper troposphere and lower stratosphere, by one horizontally and vertically circulating flow in the core of the depression suggesting a mixing of stratospheric and tropospheric air. The downward flows featured a kind of tropopause fold (Shapiro and Keyser 1990).

The conceptual picture of the 7 subsynoptic flow regimes by the model shown in Fig.7 proves to be very useful to detect the flow regimes with the associated transport of trace gases of 6-hourly ECMWF analyses, currently in use at KNMI, in cases with developing ETC's.

The obtained spatial structure and three-dimensional air flows suggest that the scales in a cyclone range from thousands of kms to tens of kms and vertically from tens of kms to hunderds

of meters. This means that only high resolution grid point models with horizontal grid distances down to tens of kms and vertical distances down to hunderds of meters are really capable to describe the observed atmospheric transport in depressions accurately. For that reason, quantitative results of the highly truncated model must be interpreted with care. For instance, diabatic effects, having impact on the mesoscale flow, are simply taking into account by a lowering of the constant static stability for the whole depression. This approach is reasonable to incorporate the release of latent heat in the ascending air on the subsynoptic scale. Concerning the descending dry air in general in the upper part of the troposphere a lowering of the static stability takes place due to stretching and in the lower troposphere and boundary layer due to destabilisation by the transport of sensible heat when the cold air moves southwards over a warm sea surface. However, the real effective value of the static stability in the descending cold air generally differ from the effective value in the ascending moist air. Indeed, daily weather maps of ECMWF with vertical velocities show that each cyclone have a couple of areas with upward and downward movements consistent in location and shape with the analytical model but the intensity of the upward velocity mostly is a factor 2 higher. This is also shown by Heijboer (1977 P.54 Fig.13) and Rogers and Bosart (1986) for the incipient, explosive and mature stage of the bomb on the North Atlantic Ocean. However, it is believed that qualitatively the three-dimensional picture found with the analytical model is not essentially changed on the subsynoptic scale. This is further confirmed by an investigation of the depression on 9 January 1991 with 6 hourly ECMWF analyses carried out by van Beeck (1991) which revealed essentially the same configuration but with weaker downdrafts.

With respect to the complete life-cycle of ETC's it has to be remarked that the observationally observed decay is not treated by the analytical model. The development is stopped by the 'quadratic' surface friction of which the constant $K_f$ in (25) linearly depends on the speed $v_m$ of the disturbance. Thus asymptotically an equilibrium is reached between the cyclone and the background flow. However, it is noted that in the core due to mixing, the thermal contrasts between the air particles decrease and the advection of the thermal vorticity by the thermal wind, being the main vorticity production term in (1), is destroyed. This process is not taken into account and should be further addressed. Another poin' is the variability of the background flow and the existence of other disturbances (cyclones and anticyclones) which can influence the behaviour of the depression. In practice, it is frequently observed that the decay of a depression is favoured when another developing young frontal wave enters the area of the old depression. The spatial structure of the background flow also influences the decay. Nonlinear accurate high resolution integrations using as initial conditions a zonal flow plus a small amplitude normal mode carried out by Simmons and Hoskins (1980) reveal that the kind of decay depends on the spatial structure of the background flow. Two characteristic life-cycles are found namely either anticyclonic wave-breaking or cyclonic cutoff at upper levels (Hoskins 1983, 1990, Thorncroft and Hoskins 1990). The solution of the analytical model shows some resemblance with the case of cyclonic cutoff.

For the calculation of the three-dimensional trajectories a nondivergent horizontal wind has been taken. It is shown by numerical integrations of quasi-geostrophic and primitive equations by Mudrick (1974), nonlinear integrations of Eady-waves by Hoskins (1976) and Hoskins and West (1979) that the advection by the divergent part of the horizontal wind is important for the development of real fronts. However, it is noted that in the semi-geostrophic version of the model ageostrophic horizontal advection is implicitly taken into account. Therefore, the essentials of the flow regimes of Fig.7 are not changed when they are translated back into the physical space. The configuration of Fig.7 is supported by the investigation of the relative

trajectories of the situation on 9 january 1991 calculated with the three-dimensional winds of the ECMWF analyses (van Beeck 1991).

The mixing between flow regimes which takes place near the bifurcation surfaces on small scales through convective and/or shear instabilities (conditional symmetric and Kelvin-Helmholtz) is not treated by the model. These processes will be further investigated on real cases based on ECMWF analyses.

Cyclones are important for the transport of air at midlatitudes. The estimated ozone transport by a depression and the total transport of ozone in one year, described in this paper, learn that ETC's are among the most important mechanisms for the transport from the stratosphere down into the troposphere.

The number of depressions in one year varies with a factor of two between different authors. More knowledge of the variability from season to season and from year to year of the number of depressions, their intensity, distribution and tracks is needed. The difference in occurrence above the oceans and above the continents has also to be explored further. This has to be done both for the Northern and the Southern Hemisphere. This variability should have consequences for the ozone budget both in the stratosphere and troposphere.

The importance of the upward flow from the boundary layer to the upper troposphere and maybe lower stratosphere, clearly revealed by the model, for the chemistry of these layers should be further explored. That boundary layer air can take part in upper tropospheric chemistry within one day after transport through an environment with clouds and precipitation, certainly has consequences for the composition of the upper troposphere.

It is not clear if the vertical transport by ETC's can be parameterized in chemical tracer models with a coarse resolution such as Moguntia (Crutzen and Zimmermann 1991). Trajectory calculations with the model suggest that the air particles in the core of the mature depression, which have been drawn in from the environment during the development, originate from very different origins partly from the low stratosphere and high troposphere in the western part of the channel and partly from the boundary layer and low free troposphere in the eastern part of the channel. That means that horizontal and vertical mixing are intertwined. This item also needs further investigation.

## 6. Acknowledgements

This work has been benefitted from discussions within the EUROTRAC/GLOMAC modelling group, from the comments of three anonymous referees and from the comments of H.Timmerman. M.J.M.Saraber of the Department of Meteorology of Wageningen Agricultural University is thanked for his valuable suggestions and for the development of the software package of the model including the graphical output with which Figs.8(a)-8(d) have been produced.

## 7. References


Anthes, R.A. 1990 Advances in the understanding and prediction of cyclone developments with limited-area fine-mesh models. In *Extratropical Cyclones, The Erik Palmen Memorial Volume,* C.W.Newton and E.O. Holopainen, Eds., Am. Met. Soc., Boston pp. 221-253

Bamber D.J., Healey,P.G.W., Jones, B.M.R., Penkett., S.A., Tuck, A.F., and Vaughan, G. 1984 Vertical profiles of tropospheric gases: chemical consequences of stratospheric intrusions. *Atm. Environ.*,**18**,1759-1766

Beeck, J.P.A.J. van 1991 Relatieve trajectorien in en rond een depressie. *Technical Report.* **TR-135.** KNMI, De Bilt (Relative trajectories in and around a depressoion, in Dutch with English Summary).

Bengtsson, L. 1990 Advances in numerical prediction of the atmospheric circulation in the extra-tropics. In *Extratropical Cyclones, The Erik Palmen Memorial Volume,* C.W.Newton and E.O. Holopainen, Eds., Am. Met. Soc., Boston pp. 193-220

Browning, K.A. 1985 Conceptual models of precipitation systems. *ESA Journal,* **9,** 157-179

Browning, K.A. 1990 Organization of cloud and precipitation in extratropical cyclones. In *Extratropical Cyclones, The Erik Palmen Memorial Volume,* C.W.Newton and E.O. Holopainen, Eds., Am. Met. Soc., Boston. pp. 129-153

Browning, K.A., and Harrold, T.W. 1970 Air motion and precipitation growth at a cold front *Quart.J.Roy.Meteor.Soc.*, **96,** 369-389

Browning, K.A., and Monk, G.A. 1982 A simple model for the synoptic analysis of cold fronts. *Quart. J. Roy. Meteor. Soc.,* **108,** 435-452

Businger, S. 1985 The synoptic climatology of polar lows outbreaks. *Tellus,* **37A,** 419-432

Businger, S. 1987 The synoptic climatology of polar-low outbreaks over the Gulf of Alaska and the Bering Sea. *Tellus*, **39A**, 307-325

Businger, S., and Reed, R.J. 1989 Cyclogenesis in cold air masses. *Weath. and Forecast.*, Vol.**4**, 133-156

Carlson, T.N. 1980 Airflow through midlatitude cyclones and the comma cloud pattern. *Mon. Weath. Rev.*, **108**, 1498-1509

Crutzen, P.J., and Zimmermann, P.R. 1991 The changing photochemistry of the troposphere. *Tellus*, **43 AB**, 136-151

Danielsen, E.F. 1968 Stratospheric tropospheric exchange based on radioactivity, ozone and potential vorticity. *J. Atmos. Sci.*, **37**, 994-1004

Dodds, I. 1971 A comparison of depressions over Europe and the North-East Atlantic . *Weather*, **26**, 210-216

Ebel, A., Hass, H., Jakobs, H.J., Laube, M., Memmesheimer, M., and Oberreuter, A. 1991 Simulation of ozone intrusion caused by a tropopause fold and cut-off low. *Atmos. Environ.*, **25A**, 2131-2144

Eliassen, A. 1990 'Transverse circulations in frontal zones'. In *Extratropical Cyclones, The Erik Palmen Memorial Volume*, C.W.Newton and E.O Holopainen, Co-Eds., Am. Met. Soc., Boston, pp. 155-165

Emanuel, K.A. and Rotunno, R. 1989 Polar lows as arctic hurricanes. *Tellus*, **41A**, 1-17

Fantini, M. 1990 The influence of heat and moisture fluxes from the ocean on the development of baroclinic waves. *J.Atmos.Sci.*, **47**, 840-855

Flierl, G.R. 1978 Models of vertical structure and the calibration of two-layer models. *Dyn.Atmos.Oceans*, **2**, 341-381

Flierl, G.R. 1979 Baroclinic solitary waves with radial symmetry. *Dyn. Atmos. Oceans*, **3**, 15-38

Flierl, G.R. 1988 On the instability of geostrophic vortices. *J.Fluid Mech.*, **197**, 349-388

Green, J.S.A., Ludlam, F.H ., and Mc Ilveen, J.F.R. 1966 Isentropic relative-flow analysis and the parcel theory. *Quart.J.Roy.Meteor.Soc.*, **92**, 210-219

Harrold, T.W. 1973 Mechanisms influencing the distribution of precipitation within baroclinic disturbances. *Quart.J.Roy. Meteor.Soc.*, **99**, 232-251

Heijboer, L.C. 1977 'Design of a baroclinic three-level quasi-geostrophic model with special emphasis on developing short frontal waves'. *Ph.D. Thesis,* University of Utrecht and KNMI Med & Verh. Publ. **102-98**, De Bilt

Heijboer, L.C. 1980 Detailstructuren in depressies; een analytisch model. Scientific Report. **W.R. 81-5**, KNMI De Bilt (A simple analytical model of the generation of meso-alpha scale phenomena in an extra-tropical cyclone,in Dutch with English summary).

Heijboer, L.C. 1980 A simple analytical model of the generation of meso-alpha scale phenomena in an extra-tropical cyclone. In Abstracts of the I.A.M.A.P. DM-6 session mesoscale phenomena: genesis and interaction. Hamburg ,7p. [copy available at KNMI from the author]

Heijboer, L.C., Timmerman, H., and van der Hoek, A. 1989 Description and performance of an hourly nowcasting and very shortrange forecasting system. *Quart.J.Roy.Meteor.Soc.*, **115**, 93-115

Hidalgo,H and Crutzen,P.J. 1977 The tropospheric and stratospheric composition perturbed by $NO_x$ emissions of high-altitude aircraft *J. Geophys. Res.* **82**, 5833-5866

Holton, J.R. 1992 *An introduction to dynamic meteorology.* Int. Geoph. Series, Vol.**48**, Acad. Press, San Diego California, Third Edition

Hoskins, B.J. 1976 Baroclinic waves and frontogenesis Part I: Introduction and Eady waves. *Quart.J.Roy.Meteor.Soc.*, **102**, 103-122

Hoskins, B.J. 1983 Dynamical processes in the atmosphere and the use of models. *Quart.J.Roy.Meteor. Soc.*, **109**, 1-21

Hoskins, B.J. 1990 Theory of extratropical cyclones. In *Extratropical Cyclones, The Erik Palmen Memorial Volume,* C.W.Newton and E.O. Holopainen, Eds., Am. Met. Soc., Boston, 63-80

Hoskins, B.J., and Bretherton, F.P. 1972 Atmospheric frontogenesis models: mathematical formulation and solution. *J. Atmos. Sci.*, **29**, 11-37

Hoskins, B.J., and Draghici, I. 1977 The forcing of ageostrophic motion according to the semi-geostrophic equations and in an isentropic coordinate model. *J.Atmos.Sci.*,**34**,1859-1867

Hoskins, B.J., McIntyre, M .E., and Robertson, A.W. 1985 On the use and significance of isentropic potential vorticity maps. *Quart.J.Roy.Meteor. Soc.*, **111**, 877-946

Hoskins, B.J., and West, N.V. 1979 Baroclinic waves and frontogenesis. Part II: Uniform potential vorticity jet flows- cold and warm fronts. *J.Atmos.Sci.*, **36**, 1663-1680

James, R.W., 1950 Theory of large-scale vortex motion in the atmosphere. Quart. J. Roy. Meteor. Soc., **76**, 255-276

Kelder, H., and Teitelbaum, H. 1991 A note on instabilities of a Kelvin-Helmholtz velocity profile in different approximations *Il Nuovo Cimento,* **14C**, 107-118..

Kletter, L. 1972 Globale Beobachtungen significanter Wirbel-strukturen. *Arch.Met.Geoph.Biokl., Ser. A,* **21**, 353-372

Komhyr, W.D., Oltmans, S.J., Franchois, P.R., Evans, W.F.J., and Matthews, W.A. 1989 The latitudinal Distribution of ozone to 35 km altitude from ECC ozonesonde observations, 1985-1987. In *Ozone in the Atmosphere.*, R.D.Bojkov and P.Fabian Eds., A.Deepak Publishing, Hampton USA, pp. 147-150

Kuo, Y.-H., Reed, R.J., and Low-Nam, S. 1991 Effects of surface energy fluxes during the early development and rapid intensification stages of seven explosive cyclones in the Western Atlantic. *Mon.Weath. Rev.*, **119**, 457-476

Ludlam, F.H. 1980 Clouds and storms, *Penn. State Univ. Press*, 405 Pp.

Mahlman, J.D., Levy II, H., and Moxim, W.J. 1980 Three-dimensional tracer structure and behaviour as simulated in two ozone precursor experiments. *J.Atmos.Sci.*, **37**, 655-685

Mansfield, D.A. 1974 Polar lows: the development of baroclinic disturbances in cold air outbreaks. *Quart. J. Roy. Meteor. Soc.*, **100**, 541-554

McWilliams, J.C. 1980 An application of equivalent modons to atmospheric blocking. *Dyn.Atmos.Oceans*, **5**, 43-66

McWilliams, J.C. and Flierl, G.R. 1979 On the evolution of isolated, nonlinear vortices. *J.Phys.Ocean.*, **9**, 1155-1182

McWilliams, J.C. and Gent, P.R. 1986 The evolution of sub-mesoscale, coherent vortices on the β-plane. *Geophys.Astrophys.Fluid Dyn.*, **35**, 235-255

Miles, M.R. 1962 Wind, temperature and humidity distribution at some cold fronts over SE. England. *Quart. J. Roy. Meteor. Soc.*, **88**, 286-300

Mudrick, S.E. 1974 A numerical study of frontogenesis. *J.Atmos.Sci.*, **31**, 869-892

Newton, C.W. 1990 Erik Palmen's contributions to the development of cyclone concepts. In *Extratropical Cyclones, The Erik Palmen Memorial Volume,* C.W.Newton and E.O. Holopainen, Eds., Am. Met. Soc., Boston, pp. 1-18

Nielsen, J.W., and Dole, R.M. 1991 A climatology of extratropical cyclones and cyclone sizes. In *First International Symposium on Winter Storms.* Am.Met.Soc., Boston, pp. 145-150

Palmen, E., and Newton, C.W. 1969 *Atmospheric circulation systems. Their structure and physical interpretation.* Int. Geoph. Series, Vol. **13,** Acad. Press, New York and London

Petterssen, S., 1956 *Weather analysis and forecasting. Vol. 1, Motion and motion systems.* McGraw-Hill, New York

Petterssen, S., and Smebye, S.J. 1971 On the development of extratropical cyclones. *Quart. J. Roy. Meteor. Soc.,* **97,** 457-482

Phillips, N. A. 1963 Geostrophic motion. *Rev. Geophys.*, **1,** 123-176

Rasmussen, E. 1979 The polar low as an extratropical CISK disturbance. *Quart. J. Roy. Meteor. Soc.,* **105,** 531-549

Rasmussen, E. 1985 A case study of a polar low development over the Barents Sea. *Tellus,* **37A,** 407-518

Reed, R.J. 1955 A study of a characteristic type of upper-level frontogenesis. *Journ. of Meteor.,* Vol.**12,** 226-237

Reed, R.J. 1990 Advances in knowledge and understanding of extratropical cyclones during the past quarter century: An overview. In *Extratropical Cyclones, The Erik Palmen Memorial Volume,* C.W.Newton and E.O Holopainen, Eds., Am. Met. Soc., Boston, pp. 27-45

Rogers, E., and Bosart, F. 1986 An investigation of explosively deepening oceanic cyclones. *Mon. Weath. Rev.*, **114**, 702-718

Sanders, F. 1986 Explosive cyclogenesis in the West-Central North Atlantic Ocean, 1981-84. Part I: Composite structure and mean behaviour. *Mon. Weath. Rev.*,**114**, 1781-1794

Sanders, F., and Gyakum, J.R. 1980 Synoptic-dynamic climatology of the "bomb". *Mon. Weath. Rev.*, **108**, 1589-1606

Shapiro, M.A. 1980 Turbulent mixing with tropopause folds as a mechanism for the exchange of chemical constituents between the stratosphere and troposphere. *J. Atmos. Sci.*, **37**, 994-1004

Shapiro, M.A., and Keyser, D.A. 1990 Fronts, jet streams and the tropopause. In *Extratropical Cyclones, The Erik Palmen Memorial Volume*, C.W.Newton and E.O. Holopainen, Eds., Am. Met. Soc., Boston, pp. 167-191

Shuman, F.G., 1957 Numerical methods in weather prediction: II. Smoothing and filtering. *Mon. Weath. Rev.*, **85**, 357-361

Simmons, A.J., and Hoskins, B.J. 1980 Barotropic influences on the growth and decay of nonlinear baroclinic waves. *J.Atmos.Sci.*, **37**, 1679-1684

Smigielski, F.J. and Mogil, H.M. 1991 Use of satellite information for improved oceanic surface analysis. In *First International Symposium on Winter Storms.* Am.Met.Soc., Boston, pp. 127-144

Turner, J., Lachlan-Cope, T., and Rasmussen, E.A. 1991 Polar lows. *Weather*, **46**, 107-114

Thorncroft, C.D., and Hoskins, B.J. 1990 Frontal cyclogenesis. *J.Atmos.Sci.*, **47**, 2317-2336

Uccellini, L.W. 1990 Processes contributing to rapid development of extratropical cyclones. In *Extratropical Cyclones, The Erik Palmen Memorial Volume,* C.W.Newton and E.O. Holopainen, Eds., Am. Met. Soc., Boston, Pp. 81-105

Uccellini, L.W., Keyser, D. Brill, K.F. and Wash, C.H. 1985 The Presidents' Day cyclone of 18-19 February 1979: Influence of upstream trough amplification and associated tropopause folding on rapid cyclogenesis. *Mon. Weath. Rev.*, **113,** 962-988

- 34 -

Vaughan, G., and Price, J.D. 1990 Ozone transport into the troposphere in a cut-off low event. In *Ozone in the atmosphere.* R.D. Bojkov & P. Fabian Eds., A.Deepak Publishing, Hampton USA, pp. 415-418

Viezee, W., Johnson, W.B., and Singh, H.B. 1983 Stratospheric ozone in the lower troposphere -2. Assesment of downward flux and ground-level impact. *Atm.Environ.*, **17,** 1979-1993

Wakamatsu, S., Uno, I., Ueda, H., Uehara K., and Tateishi, H. 1989 Observational study of stratospheric ozone intrusions into the lower troposphere. *Atm. Environ.*, **23,** 1815-1826

Warneck, P. 1988 *Chemistry of the natural atmosphere.* Int. Geoph. Series, Vol. **41,** Academic Press, New York and London, 757 pp.

## 8. Appendix

*(a) Equations for $v_m$ , $\phi_m$ and k*

The nonlinear relationships are derived with the aid of the surface integrals of the enstrophy equations for the mean flow and the thermal field.Therefor, the vorticity eqs. of the mean flow (1) and thermal field (2), formulated in the system relative frame with speed $U_m$, are multiplied by $\Delta\psi_d$ and by $\Delta\psi_T$, respectively. They read:

$$E_m \equiv E_{m1} + E_{m2} + E_{m3} + E_{m4} = 0 \tag{A1}$$

with

$$E_{m1} \equiv \partial_t\{(\Delta\psi_d{}^2)/2\}, \tag{A2}$$

$$E_{m2} \equiv J(\psi_d\ ,\ (\Delta\psi_d{}^2)/2), \tag{A3}$$

$$E_{m3} \equiv \Delta\psi_d \cdot G_1 \cdot J(\psi_T\ ,\ \Delta\psi_T), \tag{A4}$$

and

$$E_{m4} \equiv f_o \cdot K_f/dp \cdot \Delta\psi_s \cdot \Delta\psi_d. \tag{A5}$$

$$E_T \equiv E_{T1} + E_{T2} + E_{T3} + E_{T4} + E_{T5} = 0 \tag{A6}$$

with

$$E_{T1} \equiv \partial_t\{(\Delta\psi_T{}^2)/2\}, \tag{A7}$$

$$E_{T2} \equiv J(\psi_d\ ,\ (\Delta\psi_T{}^2)/2\ ), \tag{A8}$$

$$E_{T3} \equiv \Delta\psi_T \cdot J(\psi_T\ ,\ \Delta\psi_d)\ , \tag{A9}$$

$$E_{T4} \equiv -2 \cdot f_o/(dp \cdot G_2) \cdot \omega_m \cdot \Delta\psi_T\ , \tag{A10}$$

and

$$E_{T5} \equiv -\ f_o \cdot K_f/(dp \cdot G_2) . \Delta\psi_s . \Delta\psi_T. \tag{A11}$$

Defining the surface integral $I_s(f)$ as

$$I_s(f) \equiv r_m^2 \int_{r_1=0}^{\infty} \int_{\phi=0}^{2\pi} f\, r_1\, d\phi\, dr_1 \tag{A12}$$

$E_m$ and $E_T$ satisfies

$$I_s(E_m) = I_s(E_{m1}) + I_s(E_{m2}) + I_s(E_{m3}) + I_s(E_{m4}) = 0, \tag{A13}$$

and

$$I_s(E_T) = I_s(E_{T1}) + I_s(E_{T2}) + I_s(E_{T3}) + I_s(E_{T4}) + I_s(E_{T5}) = 0. \tag{A14}$$

The prognostic equation for $v_m$ and the diagnostic equation for k are obtained by the substitution of the analytic expressions for $\psi_d$ and $\psi_T$ given by (12) and (19) and the evaluation of the integrals using the formula for the integral I(p,q) defined as

$$I(p,q) \equiv \int_{r_1=0}^{\infty} r_1^{\,p} . \exp\left(-\frac{q}{2} r_1^{\,2} + \frac{q}{2}\right)\, dr_1 \tag{A15}$$

with $I(1,q) = 1/q \cdot \exp(q/2)$, (A16)

the recurrence relationship

$$I(p,q) = (p-1)/q \cdot I(p-2,q), \tag{A17}$$

and the general expression

$$I(p,q) = (p-1)/q \cdot (p-3)/q \cdot (p-5)/q \cdot \quad \cdot 2/q \cdot I(1,q), \tag{A18}$$

with integer p=3, 5, 7, .... and $q > 0$.

With the aid of (A2)-(A5), (A7)-(A11), (A12) and (A18) the surface integrals of (A13) and (A14) can be calculated and become

$$I_s(E_{m1}) = \pi \cdot r_m^2 \cdot v_m \cdot \partial_t v_m / r_m^2 \cdot 2 \cdot e, \tag{A19}$$

$$I_s(E_{m2}) = 0, \tag{A20}$$

$$I_s(E_{m3}) = - \pi \cdot r_m^2 \cdot G_1 \cdot U_T^2 \cdot v_m / r_m^3 \cdot \phi_m \cdot 3 \cdot e, \tag{A21}$$

$$I_s(E_{m4}) = \pi \cdot r_m^2 \cdot v_m^2 / r_m^2 \cdot f_o \cdot K_f / dp \cdot 2 \cdot e, \tag{A22}$$

$$I_s(E_{T1}) = \pi \cdot r_m^2 \cdot U_T^2 / r_m^2 \cdot \partial_t \phi_m \cdot (3 \cdot e \cdot \phi_m + 3/8 \cdot e^2 \cdot \phi_m^3) \tag{A23}$$

$$I_s(E_{T2}) = 0, \tag{A24}$$

$$I_s(E_{T3}) = \pi \cdot r_m^2 \cdot U_T^2 \cdot v_m / r_m^3 \cdot \phi_m \cdot 3 \cdot e, \tag{A25}$$

$$I_s(E_{T4}) = - \pi \cdot r_m^2 \cdot K_{mod} \cdot U_T^2 \cdot v_m / r_m \cdot \phi_m \cdot (1-k) \cdot e \tag{A26}$$

$$I_s(E_{T5}) = \pi \cdot r_m^2 \cdot f_o \cdot K_f / (dp \cdot G_2) \cdot U_T^2 / r_m^2 \cdot (3 \cdot e \cdot \phi_m^2 + 3/16 \cdot e^2 \cdot \phi_m^4), \tag{A27}$$

with

$$K_{mod} \equiv 4 \cdot f_o^2 / (dp^2 \cdot \sigma^* \cdot G_2). \tag{A28}$$

From (A13) the prognostic equation for $v_m$ is derived

$$\partial_t v_m = 3/2 \cdot G_1 \cdot U_T^2 / r_m \cdot \phi_m - f_o \cdot K_{fr} \cdot |v_m| / dp \cdot v_m, \tag{A29}$$

with $K_f$ dependent on $v_m$ according to

$$K_f = K_{fr} \cdot |v_m|. \tag{A30}$$

The prognostic equation for $\phi_m$ given by (23) reads

$$\partial_t \phi_m = k(t) \cdot v_m / r_m. \tag{A31}$$

From (A14) and using (A30) and (A31) the diagnostic equation for k(t) is obtained

$$k(t) = \{K_{mod} \cdot r_m^2 \cdot 3 - f_o \cdot K_{fr} / (dp \cdot G_2) \cdot r_m \cdot |v_m| / v_m \cdot (3 \cdot \phi_m + 3/16 \cdot e \cdot \phi_m^3)\}$$

$$/ (K_{mod} \cdot r_m^2 + 3 + 3/8 \cdot e \cdot \phi_m^2). \tag{A32}$$

*(b) Three-dimensional wind*

It is assumed that the complete horizontal wind rotational as well as irrotational linearly depends on p. The linear function G satisfies G=1 for $p=p_u$, G=0 for $p_m=(p_u+p_s)/2$ and G=-1 for $p=p_s$. Then using the continuity equation with the boundary conditions $\omega=0$ for $p=p_u$ and $p=p_s$ and the demand that the integral of G from $p_u$ to $p_s$ is zero, it follows that

$$\nabla \cdot \mathbf{V}_m = 0. \tag{A33}$$

The vertical velocity $\omega$ satisfies

$$\omega = (\nabla \cdot \mathbf{V}_T) \cdot \int G(p)dp \tag{A34}$$

and the vertically averaged $\omega$

$$\omega_m = (\nabla \cdot \mathbf{V}_T)/(p_s - p_u) \cdot \int[\int\{G(p)dp\}]dp. \tag{A35}$$

It is shown using (A34) and (A35) that

$$\omega = 3/2 \cdot (1 - p_1^2) \cdot \omega_m \tag{A36}$$

with a dimensionless pressure coordinate $p_1$

$$p_1 \equiv - G(p) = 2 \cdot (p - p_m)/(p_s - p_u). \tag{A37}$$

For the computation of the horizontal wind components u and v the rotational part is taken, satisfying:

$$u = u_m(x,y,t) - p_1 \cdot u_T(x,y,t), \tag{A38}$$

$$v = v_m(x,y,t) - p_1 \cdot v_T(x,y,t). \tag{A39}$$

Dimensionless coordinates $x_1$ and $y_1$ are introduced as

$$x_1 \equiv (x - U_m \cdot t)/r_m, \quad y_1 \equiv y/r_m \quad \text{with} \quad x_1 = r_1 \cdot \cos\phi, \quad y_1 = r_1 \cdot \sin\phi. \tag{A40}$$

$r_1$ satisfies

$$r_1 = \sqrt{(x_1^2 + y_1^2)}. \tag{A41}$$

With the aid of (11) and (A40) it is shown that

$$u_m = - \partial_y \psi_m = U_m - 1/r_m \cdot \partial_{y1} \psi_d, \tag{A42}$$

$$v_m = \partial_x \psi_m = 1/r_m \cdot \partial_{x1} \psi_d. \tag{A43}$$

The components of the thermal wind can be written as

$$u_T = - \partial_y \psi_T = - \partial_{y1} \psi_T = -1/r_m \cdot \partial_{y1} \psi_T, \tag{A44}$$

$$v_T = \partial_x \psi_T = \partial_{x1} \psi_T = 1/r_m \cdot \partial_{x1} \psi_T. \tag{A45}$$

Using (14) it easily follows that

$$\partial_{x1} E = -x_1 \cdot E, \quad \partial_{y1} E = -y_1 \cdot E. \tag{A46}$$

Defining the quantity H as

$$H \equiv E \cdot \phi_m, \tag{A47}$$

one obtains from (A46)

$$\partial_{x1} H = -x_1 . H, \quad \partial_{y1} H = -y_1 \cdot H. \tag{A48}$$

Now taking (19), (21) and (22) and using (A40) $\psi_T$ is expressed as

$$\psi_T = r_m \cdot (-U_T \cdot y_1 \cdot \cos H + U_T \cdot x_1 \cdot \sin H). \tag{A49}$$

From (12), (17), (19), (21), (22), (A36), (A37), (A42)-(A45) the three dimensional wind consisting of u-, v- and $\omega$-components reads

$$u(x_1, y_1, p_1, t) = U_m - v_m \cdot y_1 \cdot E - p_1 \cdot \{U_T \cdot (x_1 \cdot y_1 \cdot H + 1) \cdot \cos H + U_T \cdot y_1^2 \cdot H \cdot \sin H\}, \tag{A50}$$

$$v(x_1, y_1, p_1, t) = V_m + v_m \cdot x_1 \cdot E + p_1 \cdot \{U_T \cdot (x_1 \cdot y_1 \cdot H - 1) \cdot \sin H + U_T \cdot x_1^2 \cdot H \cdot \cos H\}, \tag{A51}$$

$$\omega(x_1, y_1, p_1, t) = -3 \cdot f_o \cdot (1 - p_1^2) / (\sigma^* \cdot dp) \cdot (1 - k) \cdot v_m \cdot U_T \cdot E \cdot (x_1 \cdot \cos H - y_1 \cdot \sin H). \tag{A52}$$

## Figure Captions

Figure 1(a).
Wave in the thermal field associated with rows of circular cyclones and anticyclones for small $\phi_m$ and $v_m$ ($\psi_d$ thinly drawn, $\psi_T$ bold).

Figure 1(b).
As Fig.1(b) but for a rectangular sine-wave with $L_y=2 \cdot L_x$ and $L_x=4 \cdot r_m$.

Figure 2.
Relationship between the average values of the static stability $\sigma_{s.ad.}$ for the layer 300-850 mb as function of the saturated potential temperature $\theta_s$ at 1000 mb.

Figure 3.
Numerically computed heigth $z_s$ of 1000 mb (bold), thermal field $z_T$ (solid), and vertical velocity $\omega_m$ (dashed) valid for t = 6 hours using Eqs. (1), (2) and (3). Contour intervals are 40 m for $z_T$ and $z_s$, respectively and 50 mb/12hrs for $\omega_m$.

Figure 4.
Comparison of the analytical model with the numerical model VIMOLA.
Composite of numerically computed $z_s$ (bold), $z_T$ (solid) and $\omega_m$ (dashed) valid for t = 18 hours. Contour intervals are 20 m for $z_s$ and $z_T$, respectively and 50 mb/12 hrs for $\omega_m$.
(a) Numerical model VIMOLA. (b) Analytical model.

Figure 5(a).
Computed central pressure fall during 24 hours at sea level according to Eqs. (24) and (26) of the analytic solution starting from the initial values $\phi_m = 0^0$ and $v_m = 1$ m s$^{-1}$ with values of the background flow $U_T = 10$ m s$^{-1}$ and $\sigma^* = 2.2 \times 10^{-7}$ kg$^{-2}$ m$^4$ s$^{-2}$ (solid), $U_T = 14$ m s$^{-1}$ and $\sigma^* = 6.5 \times 10^{-7}$ kg$^{-2}$ m$^4$ s$^{-2}$ at the most unstable radius $r_m$ (dashed dotted) and $U_T = 10$ m s$^{-1}$ and $\sigma^* = 6.5 \times 10^{-7}$ kg$^{-2}$ m$^4$ s$^{-2}$ at the most unstable radius $r_m$ (dashed). Bold dashed is the threshold 1 Bergeron at $45^0$ N.

Figure 5(b).
As Fig. 5(a) but for the maximum wind speed $v_m$ of the circular disturbance.

Figure 5(c).
As Fig. 5(c) but for the angle $\phi_m$ at which the thermal field is wrapped up by the circular disturbance.

Figure 6.
Trajectories of the solution in the $\phi_m$ - $v_m$ space determined by (24) and (26) for $r_m = 500$ km, $U_T = 10$ m s$^{-1}$ and $\sigma^* = 2.2 \times 10^{-7}$ kg$^{-2}$ m$^4$ s$^{-2}$. The positive $\phi_m$-axis corresponds to the A-development and the positive $v_m$-axis to the B-development (Petterssen and Smebye 1971).

Figure 7.
Three-dimensional qualitative view of the seven subsynoptic relative flow regimes according to the calculation of relative streamlines of the cyclone of the analytical model. The channel is directed from west to east and bounded by 200 mb and 1000 mb (solid streamlines). The intersection of the vertical cross-section at the eastern and western sides of the channel with the bifurcation surfaces, separating the flows, is denoted by bold solid lines.The tropopause of the model is indicated by the straight bold line at the western side of the channel.

Figure 8.
Isobars (thick solid) and isotherms (thin lines) by the analytical model at the lowest level ($p=p_s$) starting with straight isotherms and a circular disturbance.
(a) t=0 hours. (b) t=12 hours. (c) t=24 hours. (d) t=36 hours.

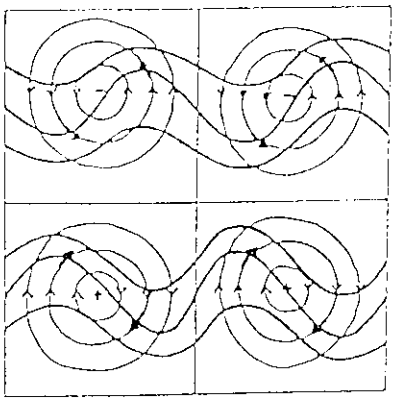

Figure 1(a).

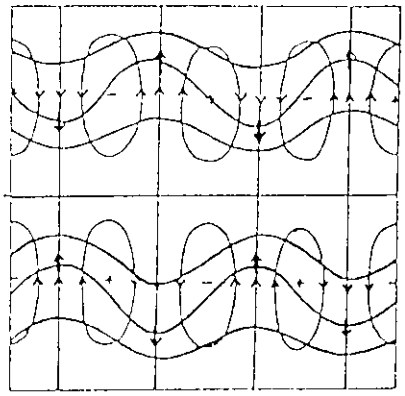

Figure 1(b).

Figure 1(a).
Wave in the thermal field associated with rows of circular cyclones and anticyclones for small $\varphi_m$ and $v_m$ ($\psi_d$ thinly drawn, $\psi_T$ bold).

Figure 1(b).
As Fig.1(b) but for a rectangular sine-wave with $L_y = 2 \cdot L_x$ and $L_x = 4 \cdot r_m$.

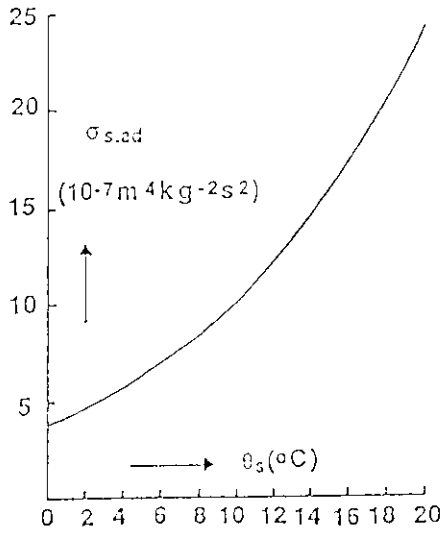


Figure 2.

Figure 2.

Relationship between the average values of the static stability $\sigma_{s.ad.}$ for the layer 300-850 mb as function of the saturated potential temperature $\theta_s$ at 1000 mb.

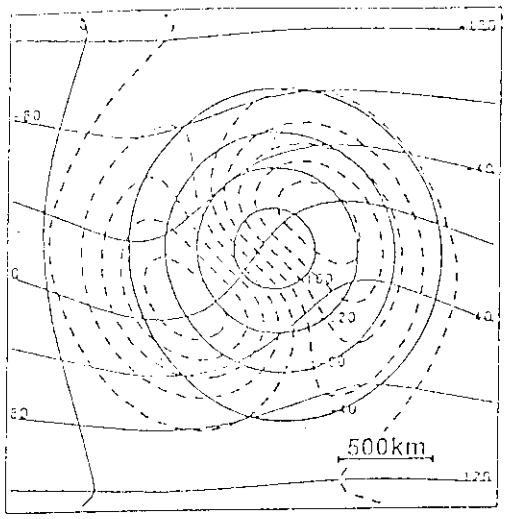


Figure 3.

Figure 3.

Numerically computed heigth $z_s$ of 1000 mb (bold), thermal field $z_T$ (solid), and vertical velocity $\omega_m$ (dashed) valid for t = 6 hours using Eqs. (1), (2) and (3). Contour intervals are 40 m for $z_T$ and $z_s$, respectively and 50 mb/12hrs for $\omega_m$.

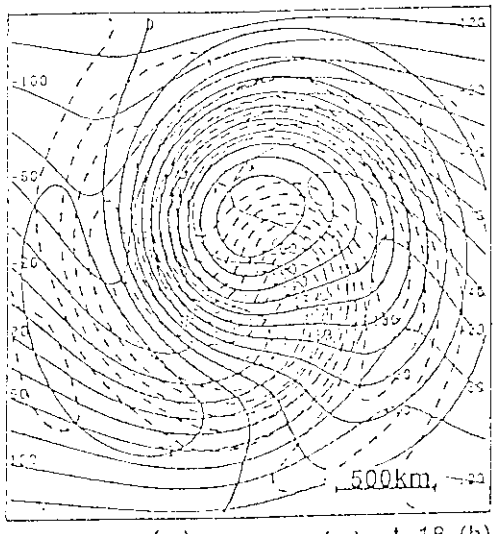


Figure 4(a).

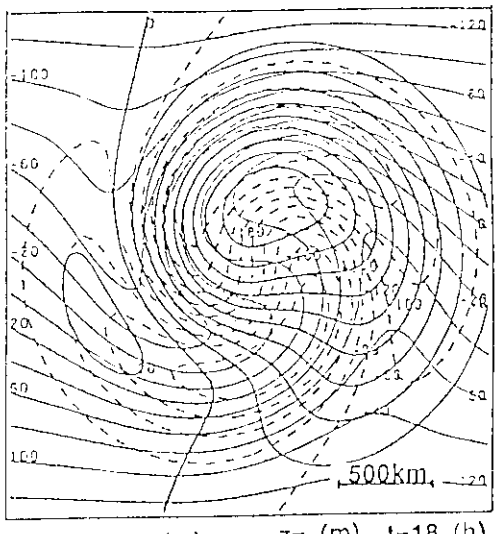


Figure 4(b).

Figure 4(a).

Composite of numerically computed $z_s$ (bold), $z_T$ (solid) and $\omega_m$ (dashed) valid for t = 18 hours. Contour intervals are 20 m for $z_s$ and $z_T$, respectively and 50 mb/12 hrs for $\omega_m$.

Figure 4(b).

As Fig. 4(a) but for the analytic solution.

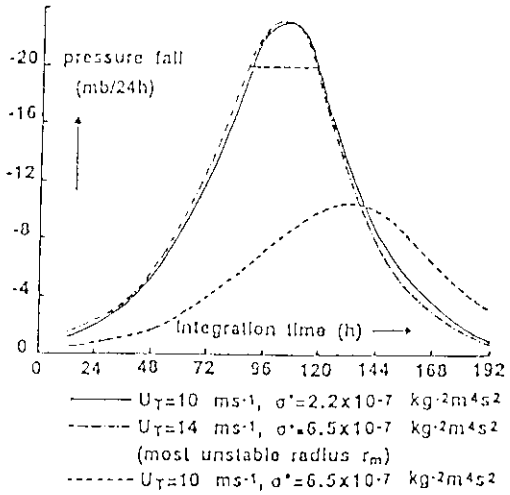


Figure 5(a).

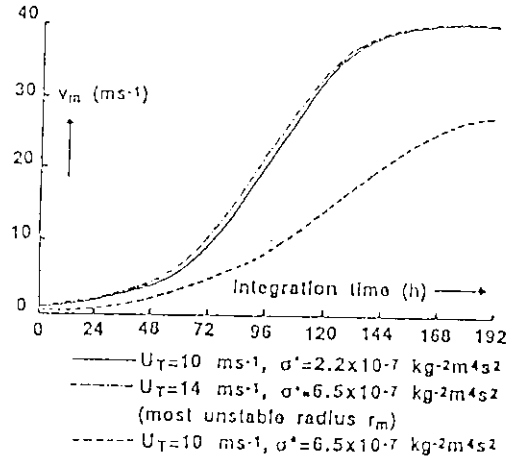


Figure 5(b).

Figure 5(a).
Computed central pressure fall during 24 hours at sea level according to Eqs. (24) and (26) of the analytic solution starting from the initial values $\phi_m = 0^0$ and $v_m = 1$ m s$^{-1}$ with values of the background flow $U_T = 10$ m s$^{-1}$ and $\sigma^* = 2.2\text{x}10^{-7}$ kg$^{-2}$ m$^4$ s$^{-2}$ (solid), $U_T = 14$ m s$^{-1}$ and $\sigma^* = 6.5\text{x}10^{-7}$ kg$^{-2}$ m$^4$ s$^{-2}$ at the most unstable radius $r_m$ (dashed dotted) and $U_T = 10$ m s$^{-1}$ and $\sigma^* = 6.5\text{x}10^{-7}$ kg$^{-2}$ m$^4$ s$^{-2}$ at the most unstable radius $r_m$ (dashed). Bold dashed is the threshold 1 Bergeron at 45$^0$ N.

Figure 5(b).
As Fig. 5(a) but for the maximum wind speed $v_m$ of the circular disturbance.

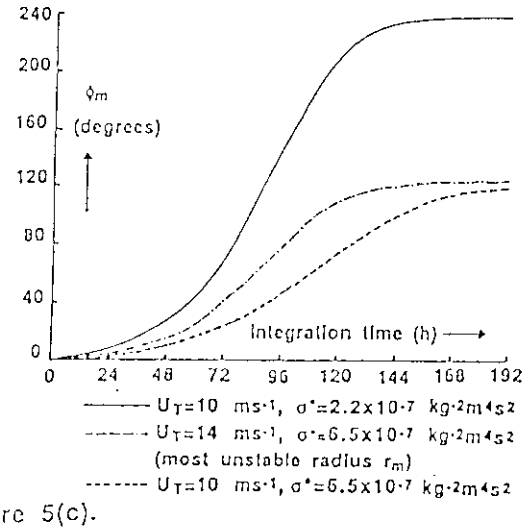


Figure 5(c).

Figure 5(c).
As Fig. 5(c) but for the angle $\phi_m$ at which the thermal field is wrapped up by the circular disturbance.

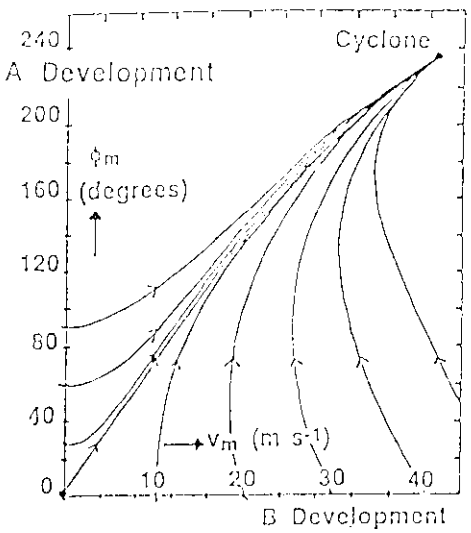


Figure 6.

Figure 6.

Trajectories of the solution in the $\phi_m$ . $v_m$ space determined by (24) and (26) for $r_m$ = 500 km, $U_T$ = 10 m s$^{-1}$ and $\sigma^*$ = 2.2x10$^{-7}$ kg$^{-2}$ m$^4$ s$^{-2}$. The positive $\phi_m$-axis corresponds to the A-development and the positive $v_m$-axis to the B-development (Petterssen and Smebye 1971).

Relative trajectories within and around a standard moving extratropical cyclone

1 Warm moist conveyor belt
2 Low tropospheric flow of the environment
3 Cold moist conveyor belt
4 Descending stratospheric air overrunning the warm moist conveyor belt
5 Stratospheric flow of the environment
6 Descending stratospheric air into the troposphere
7 Circulating air in the centre of the depression moving with the speed of the depression

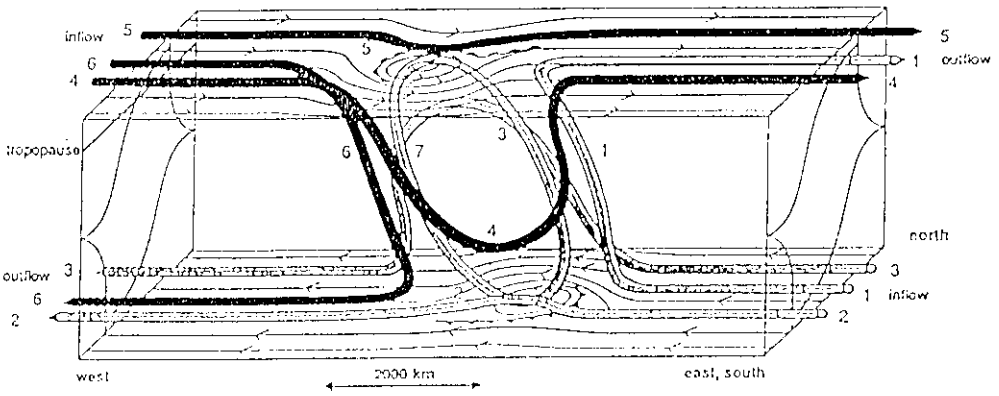


Figure 7.

Figure 7.

Three-dimensional qualitative view of the seven subsynoptic relative flow regimes according to the calculation of relative streamlines of the cyclone of the analytical model. The channel is directed from west to east and bounded by 200 mb and 1000 mb (solid streamlines). The intersection of the vertical cross-section at the eastern and western sides of the channel with the bifurcation surfaces, separating the flows, is denoted by bold solid lines.The tropopause of the model is indicated by the straight bold line at the western side of the channel.

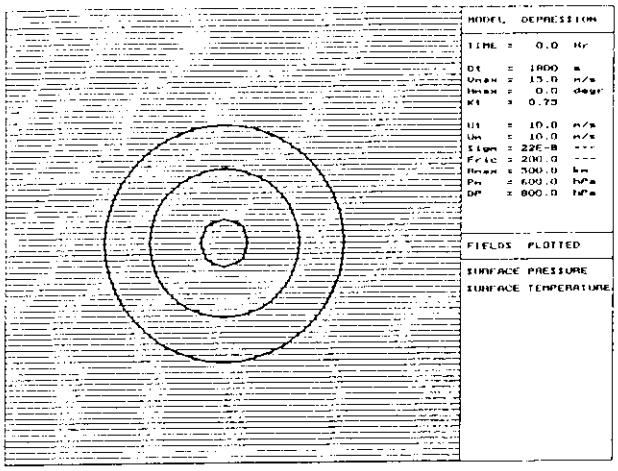


Figure 8(a).

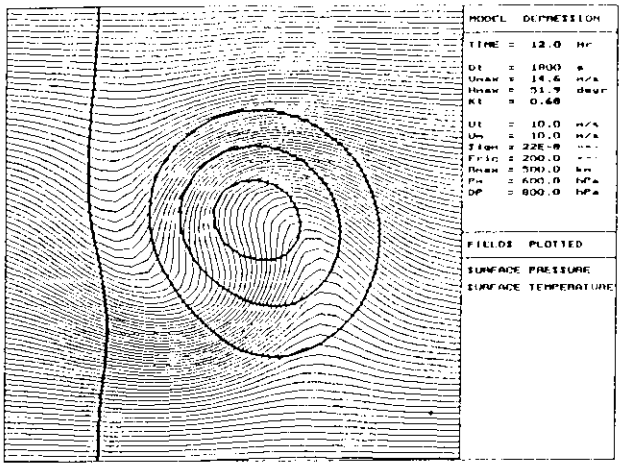


Figure 8(b).

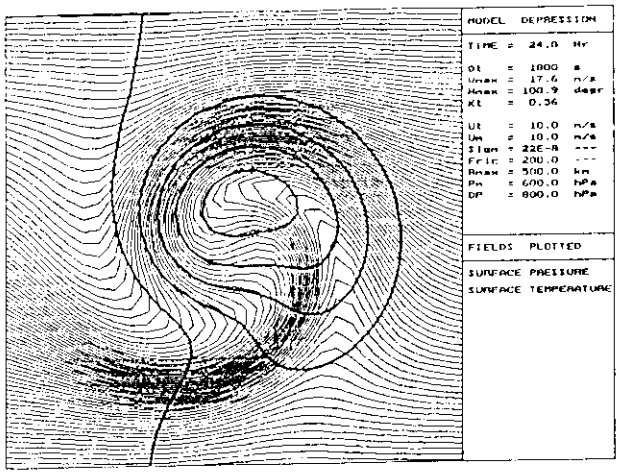


Figure 8(c).

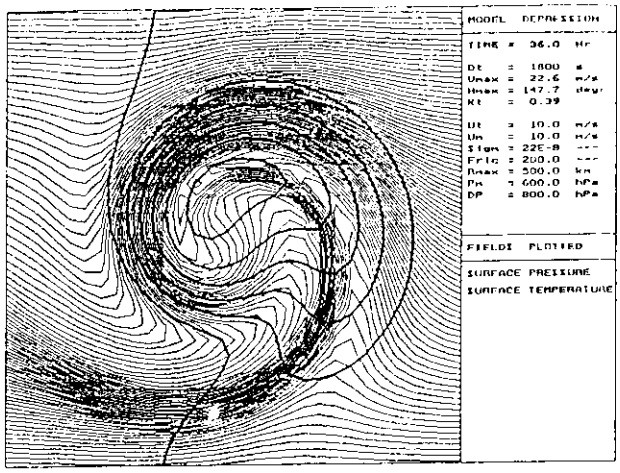


Figure 8(d).

**Figure 8.**

Figure 8.

Isobars (thick solid) and isotherms (thin lines) by the analytical model at the lowest level ($p=p_s$) starting with straight isotherms ($U_T$= 10 ms$^{-1}$) and a circular disturbance ($v_m$ = 15 ms$^{-1}$).

(a) t=0 hours. (b) t=12 hours. (c) t=24 hours.(d) t=36 hours.